Supplementary Information for

Visualizing Side-chains of Invisible Protein Conformers by Solution NMR

Guillaume Bouvignies[1], Pramodh Vallurupalli[1], and Lewis E. Kay[1,2]

[1]Departments of Molecular Genetics, Biochemistry and Chemistry, The University of Toronto, Toronto, Ontario, M5S 1A8, Canada

[2]Hospital for Sick Children, Program in Molecular Structure and Function, 555 University Avenue, Toronto, Ontario, M5G 1X8, Canada

Simulations to establish the robustness of CEST data. In order to understand the inherent limitations of the CEST experiment, in particular how the rate of chemical exchange influences extracted p_E and k_{ex} parameters as well as $\Delta\varpi$ values, we have carried out a series of computations based on some of the experimental data sets that have been recorded and analyzed in the present study. The computations are based on a subset of residues of the Fyn SH3 domain, including Y10, L18, I28, K25, W36, T43, I50 and P51 (corresponding to 39 CEST profiles), with nucleus specific values of ^{13}C R_1, ^{13}C R_2, $\Delta\varpi$ and uncertainties in I/I_o (varying from 0.1 - 2.9%, depending on the nucleus) taken from experiment. A series of data sets have been simulated, with each data set comprising CEST profiles for each ^{13}C position of the residues listed above, using p_E = 2.5%. The effects of one-bond ^{13}C-^{13}C scalar couplings have also been included by simulating individual multiplet components and then adding all of the components to produce the profile. Noise has been added to each of the computed CEST profiles by assuming that the calculated uncertainties in I/I_o values based on experiment define the standard deviation of a Gaussian distribution of the error in the data. A series of simulated data sets was constructed with k_{ex} chosen from {100 s^{-1}, 400 s^{-1}, 800 s^{-1}, 1200 s^{-1}}. Simulations of CEST profiles were performed assuming a two-site chemical exchange model with magnetization evolution described by the Bloch-McConnell equations[1]. A value of T_{CEST} = 250 ms and a CEST B_1 field = 23 Hz have been used in the simulations, identical to those in the experiment recorded on the SH3 domain. Each of the simulated data sets was then fit in a manner analogous to the experimental data and the values of p_E, k_{ex}, $\Delta\varpi$ tabulated. The process was repeated 500 times for each data set with noise added as described above. The distribution of p_E, k_{ex} values so obtained is plotted in Supplementary Figure 6a for k_{ex} = 100 s^{-1} (red), 400 s^{-1} (blue), 800 s^{-1} (green) and 1200 s^{-1} (purple). In addition, the

standard deviations between the extracted and input $\Delta\varpi$ values, $\Delta\Delta\varpi$, (corresponding to the errors in fitted $\Delta\varpi$ values) are plotted in Supplementary Figure 6e separated into 4 classes of $\Delta\varpi$ (according to < 1 ppm, 1ppm-2ppm, 2ppm-3ppm, 3ppm-4ppm) for each of the input k_{ex} values (color coded as for Supplementary Figure 6a). Thus, errors in extracted $\Delta\varpi$ values within each of the four $\Delta\varpi$ classes listed above can be read from the histogram, with red values corresponding to k_{ex} = 100 s^{-1}, blue k_{ex} = 400 s^{-1}, etc. These calculations have then been repeated by omitting all CEST profiles with $\Delta\varpi$ > 3 ppm to generate Figures 6b,f, eliminating data corresponding to $\Delta\varpi$ > 2 ppm to generate Figures 6c,g, and finally eliminating data corresponding to $\Delta\varpi$ > 1 ppm to produce Figures 6d,h. In this manner the sensitivity of the extracted parameters to the sizes of the chemical shift differences in the exchanging system can be evaluated.

It is important to emphasize that the results of Supplementary Figure 6 reflect the input signal to noise, distribution of $\Delta\varpi$ values and p_E that have been used in the simulations and these will vary with each experimental system studied. It is not possible to simulate every situation here. Nevertheless, important trends emerge from this analysis that are likely general. First, Figure 6a shows that so long as the fitted data includes large $\Delta\varpi$ values (*i.e.*, major and minor state dips are resolved; in this case $\Delta\varpi$ is as large as 4 ppm), accurate values of p_E and k_{ex} can be fit from CEST profiles. The accuracy and precision remain quite high even as k_{ex} increases to 1200 s^{-1} (purple in Supplementary Figure 6a). Accurate values of p_E and k_{ex} are still obtained when profiles corresponding to $\Delta\varpi$ > 3 ppm are removed from data sets (Supplementary Information Figure 6b). A slight decrease in accuracy is observed once profiles with $\Delta\varpi$ > 2 ppm are removed, especially for k_{ex} = 800 s^{-1}, 1200 s^{-1} (6c). Once $\Delta\varpi$ values > 1 ppm are removed, exchange parameters become less well defined (6d), irrespective of k_{ex}. This is due to the fact that the minor

and major state dips are no longer resolved. Second, extracted chemical shift differences are, in general, robustly determined and often more so than p_E and k_{ex} values (especially when only small $\Delta\varpi$ values are considered). Third in all cases, $\Delta\varpi$ values are more accurately determined when k_{ex} is smallest since then the dips from the excited state are most narrow (note the trend of red, blue, green and purple in order of increasing $\Delta\Delta\varpi$ in each of the $\Delta\varpi$ classes, 6e-h). Fourth, in general, it is not possible to conclude that $\Delta\varpi$ values become more accurately determined as $\Delta\varpi$ increases. For example, for large $\Delta\varpi$ values, for which separate dips corresponding to ground and excited states are observed, the determining factor is signal to noise that can vary significantly for different nuclei. As a final note, we have carried out the simulations described above using only a subset of the residues initially selected, and obtained the same general trends. Thus, the overall conclusions based on the computations are likely to be general, however the specific details will of course vary with each system considered.

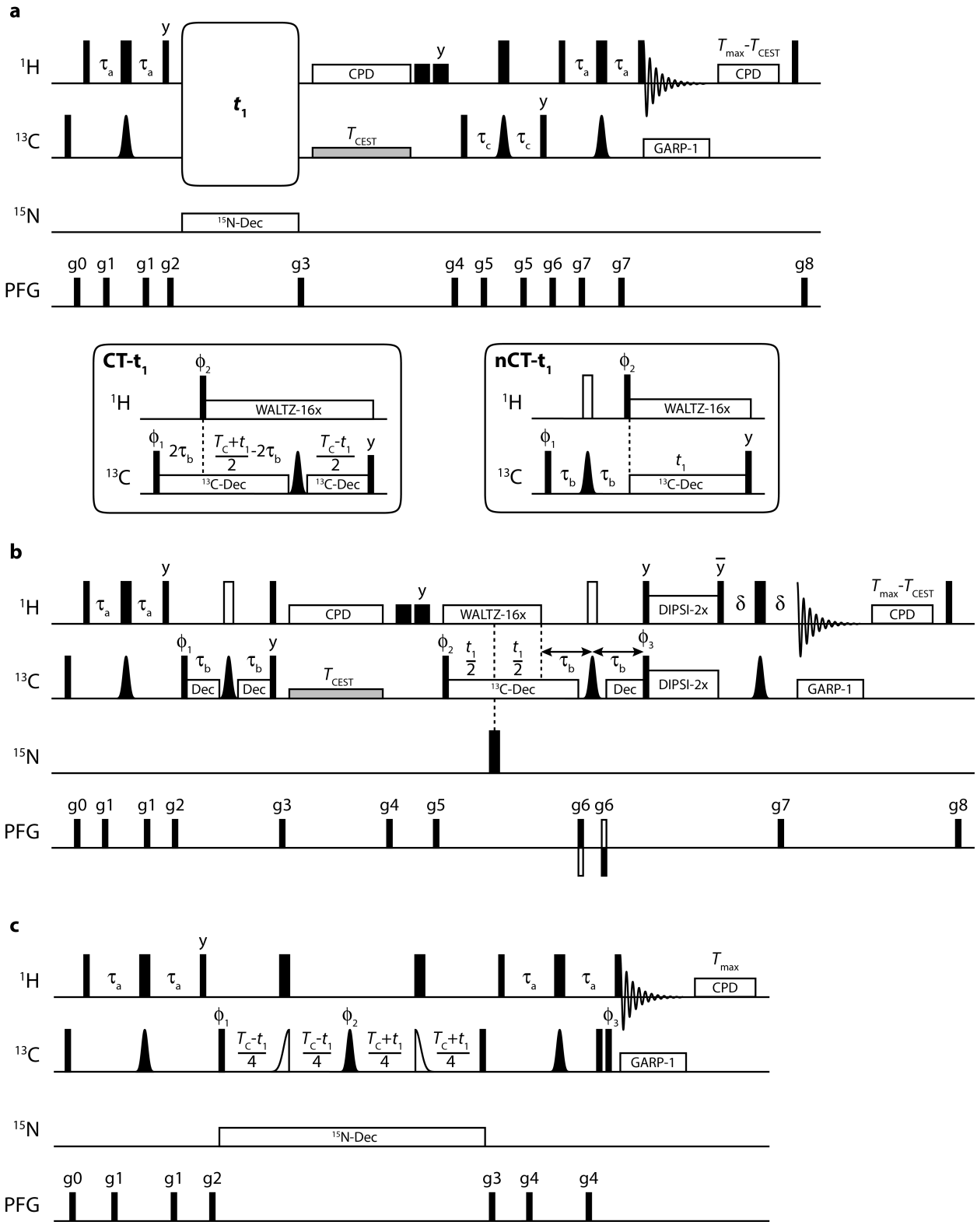
a
^{1}H
^{13}C
^{15}N
PFG
τ_a
τ_b
τ_c
y
t_1
CPD
T_{CEST}
GARP-1
^{15}N-Dec
T_{max}-T_{CEST}
g0 g1 g1 g2 g3 g4 g5 g5 g6 g7 g7 g8
CT-t_1
ϕ_2
WALTZ-16x
ϕ_1
$2\tau_b$
$\frac{T_c+t_1}{2}-2\tau_b$
$\frac{T_c-t_1}{2}$
^{13}C-Dec
nCT-t_1
b
$\bar{y}$
DIPSI-2x
δ
ϕ_3
Dec
$\frac{t_1}{2}$
c
$\frac{T_c-t_1}{4}$
$\frac{T_c+t_1}{4}$
T_{max}

Supplementary Figure 1. Pulse schemes for measurement of excited state aliphatic ^{13}C chemical shifts in uniformly ^{13}C labeled proteins. (**a**) ^{13}C CEST experiment for measuring all aliphatic side-chain ^{13}C chemical shifts in the excited state, including backbone $^{13}C^{\alpha}$ shifts of Gly and Ser (all other $^{13}C^{\alpha}$ shifts are obtained from scheme b). Shown in the insets are constant-time[2; 3] (CT-t_1) and non constant-time (nCT-t_1) versions of the experiment that are used for measurement of shifts of the residues indicated in Supplementary Table 1. ^{1}H and ^{13}C 90° (180°) rectangular RF pulses are shown as narrow (wide) black bars; $90_x180_y90_x$ composite pulses[4] are indicated by white rectangles. The ^{1}H carrier is placed on the water signal for the duration of the experiment with the exception of the CEST period when it is centered in the proton region of interest (for example, ~ 1 ppm when ^{13}C methyl chemical shifts of the excited state are measured). In a similar manner the ^{13}C carrier is placed at 36 ppm, until the CEST interval when it is moved to the desired frequency. Subsequently, the carrier is returned to 36 ppm until acquisition when it is centered in the region to be decoupled. The ^{15}N carrier is positioned at 119 ppm with decoupling achieved over the bandwidths listed in Supplementary Table 1. All pulse phases are assumed to be x, unless indicated otherwise. ^{1}H and ^{13}C rectangular pulses are applied at the highest possible power level unless indicated otherwise. ^{1}H decoupling during the CEST interval is achieved using a $90_x240_y90_x$ scheme, as discussed previously[5], using a 3 kHz field (at 14 T), while decoupling during t_1 evolution proceeds with a 5.5 kHz WALTZ-16 field[6]. Dephasing of water is partially achieved through the application of an x(2ms),y(3 ms) pulse pair immediately following the CEST interval using a 3 kHz field. Shaped ^{13}C pulses are applied using a REBURP profile[7] centered at 40 ppm, with refocusing (inversion) over the complete aliphatic bandwidth. ^{13}C decoupling during t_1 is achieved using constant adiabaticity schemes[8; 9]. In the case of aliphatic ^{13}C decoupling a pair of fields are typically employed, swept in opposite directions and applied symmetrically about the region of interest so as to minimize artifacts[10; 11]. For example, when chemical shifts in the range 27.2-47.1 ppm are measured ('region of interest'), the decoupling field is centered at 145 ppm and swept upfield from 190 ppm to 100 ppm, with a second field centered at -73 ppm, and swept downfield from -118 ppm to -28 ppm. The first swept field decouples aromatics and carbonyls, while the second field compensates the first. Details are provided in Supplementary Table 1. ^{13}C decoupling during acquisition is achieved using a 2 kHz GARP-1 field (14 T)[12]. During the CEST interval a ^{13}C B_1 field on the order of 15-50 Hz is

typically used. Delays used are: τ_a = 1.85 ms; τ_b = τ_c =1.85 ms (for AX spin systems), τ_b = τ_c =0.925 ms (AX_2), τ_b =1.217 ms and τ_c = 0.784 ms (AX_3), T_C=1/J_{CC} ~ 28 ms. Values of T_{CEST} are typically between 200-700 ms. A ^{1}H decoupling block of length T_{max} – T_{CEST} (where T_{max} is the maximum T_{CEST} delay used) is applied at the end of acquisition so that the extent of heating is constant over all measurements, including for the data set recorded with T_{CEST} = 0. The final ^{1}H 90^o pulse ensures that ^{1}H magnetization relaxes back to equilibrium for the same time for T_{CEST}=0,≠0. A recycle delay of 1.5 was used between scans. The phase cycle is: ϕ1=2(x),2(-x), ϕ2=y,-y, rec=2(x),2(-x). Quadrature in F_1 is achieved via States-TPPI[13] of ϕ1. Gradient strengths G/cm(length in ms) are: g0=16(0.5), g1=10(0.25), g2=-25(1), g3=-40(1), g4=30(0.5), g5=20(0.2), g6=20(0.8), g7=-36(0.3), g8=16(0.25).

(**b**) Enhanced sensitivity based ^{13}C CEST pulse scheme for measurement of $^{13}C^{\alpha}$ chemical shifts in the excited state (AX spin systems). Many of the details are similar to what has been described in (**a**) and will not be repeated here. The ^{13}C carrier is placed at 58 ppm for the duration of the sequence, with the exception of the T_{CEST} period when it is moved to the desired frequency. Details of ^{13}C decoupling during t_1 are given in Supplementary Table 1. Quadrature detection during t_1 is achieved using an enhanced sensitivity based approach[14; 15] whereby cosine and sine modulated components are transferred back to ^{1}H for detection using a planar TOCSY scheme[16]. For each t_1 point a pair of FIDs is recorded corresponding to (ϕ3,g6) and (ϕ3+π,-g6) and stored separately for post-acquisition processing. An 8kHz DIPSI-2 mixing scheme[17] (of length corresponding to approximately 1/J_{CH}, where J_{CH} is the one bond ^{13}C-^{1}H scalar coupling) is used for the TOCSY transfer. Values of τ_a and τ_b are set to 1.8 ms, δ = g7+0.3 ms. The phase cycle is: ϕ1=x,-x, ϕ2=2(y),2(-y), ϕ3=y, rec=x,2(-x),x. Gradient strengths G/cm(length in ms) are: g0=15(1), g1=20(0.5), g2=30(0.8), g3=-32(1), g4=-20(0.7), g5=-20(0.9), g6=30(0.2), g7=29.6(0.1), g8=16(0.5).

(**c**) Pulse scheme for measurement of ^{13}C chemical shifts (ground state) that are subsequently used in fits of CEST profiles. ^{13}C decoupling in t_1 can introduce Bloch Siegert shifts[18] and is therefore not employed. Instead scalar coupled evolution due to one-bond interactions with carbonyl and aromatic carbons is refocused by the application of the shaped (white) pulses shown (IBURP-2 profiles[7], with bandwidths extending from ~ 105-185 ppm; 300 μs pulse widths

at 14.0T). Many other details are as in (**a**) and are not repeated. A WURST-2 ^{15}N field[19] that decouples backbone amides and amines of Lys (30-40 ppm) and Arg (80-90 ppm) is employed during t_1. Values of τ_a = 1.85 ms, $T_C=1/J_{CC}$ ~ 28 ms are used. The phase cycle is: $\phi1$=x, $\phi2$=x,y,-x,-y, $\phi3$=2(x),2(-x), rec=x,-x. Gradient strengths G/cm(length in ms) are: g0=10(0.5), g1=6(0.3), g2=30(1.5), g3=20(0.6), g4=4(0.2).

Supplementary Figure 2. ^{13}C CEST profiles for each residue of the G48A Fyn SH3 domain, 25°C, 14.0T.

S1

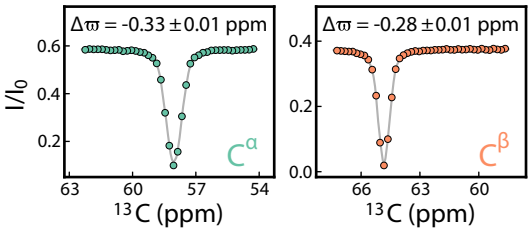

T2

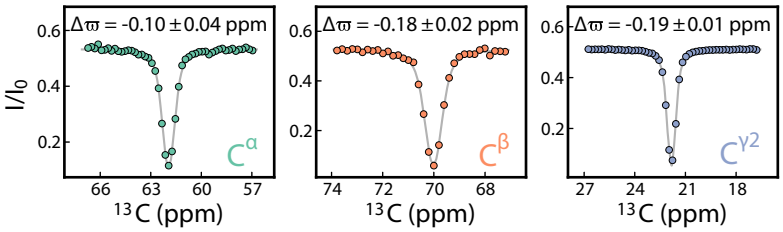

L3

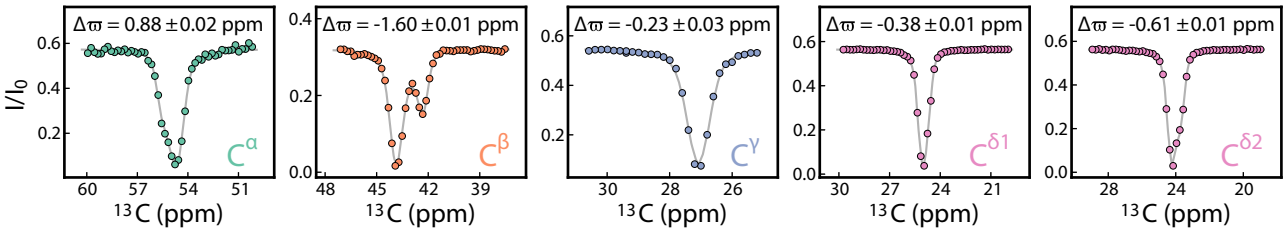

F4

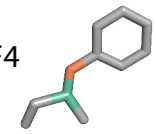

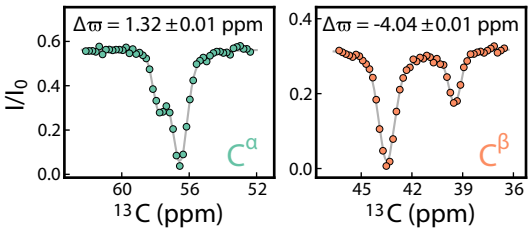

E5

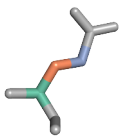

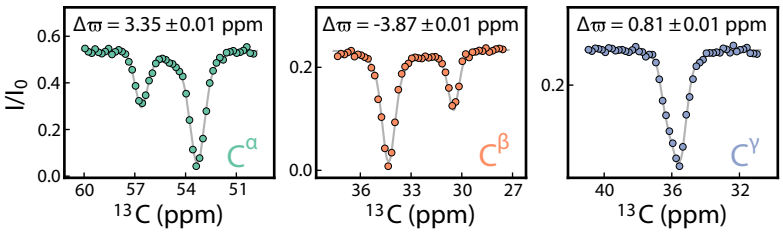

A6

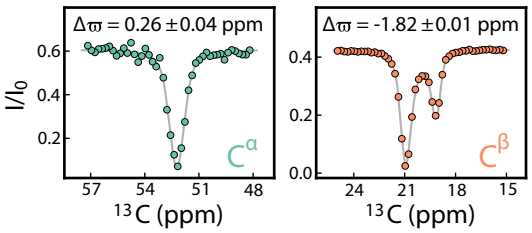

L7

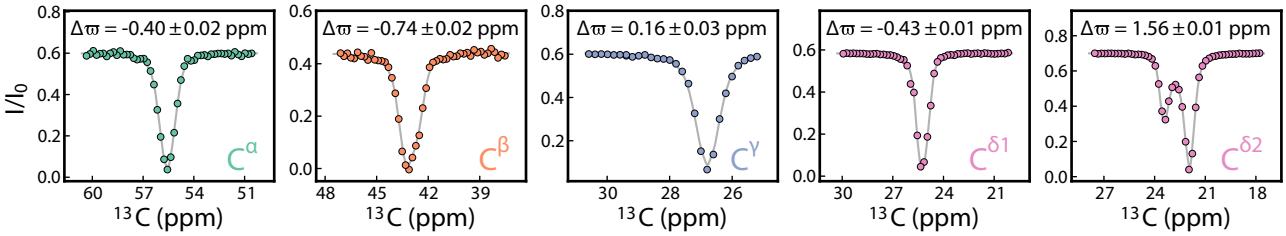

Y8

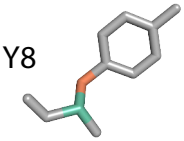

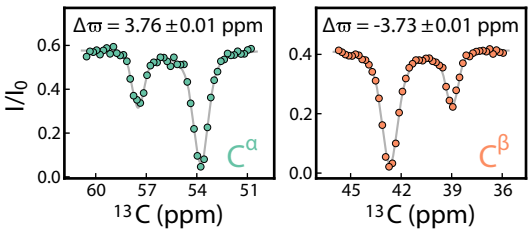

D9

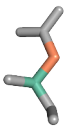

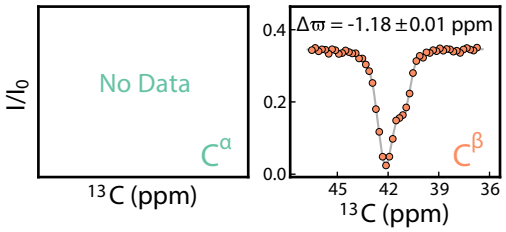

Y10

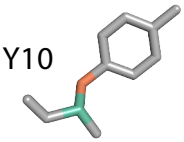

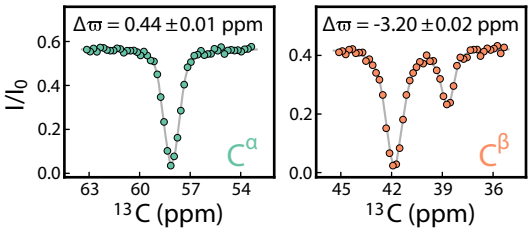

E11

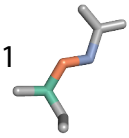

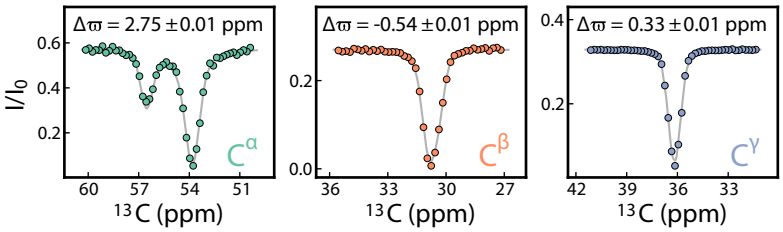

A12

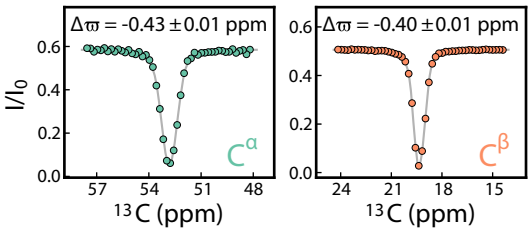

R13

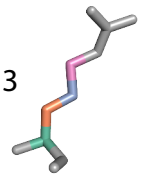

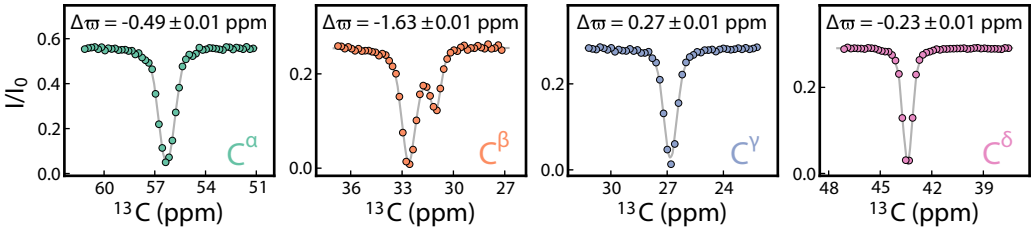

T14

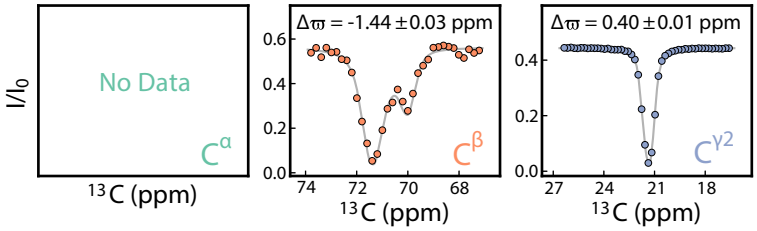

E15

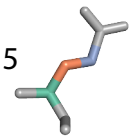

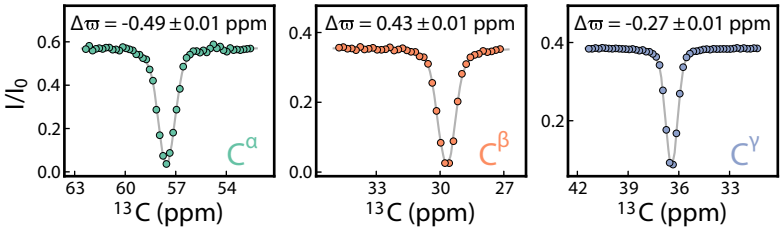

D16

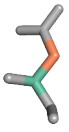

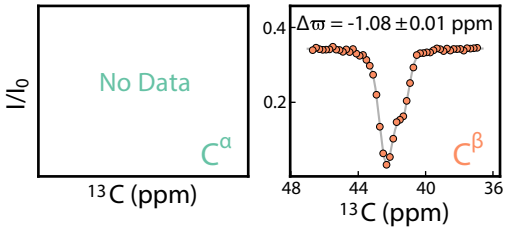

D17

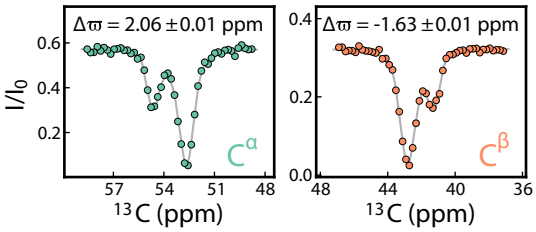

L18

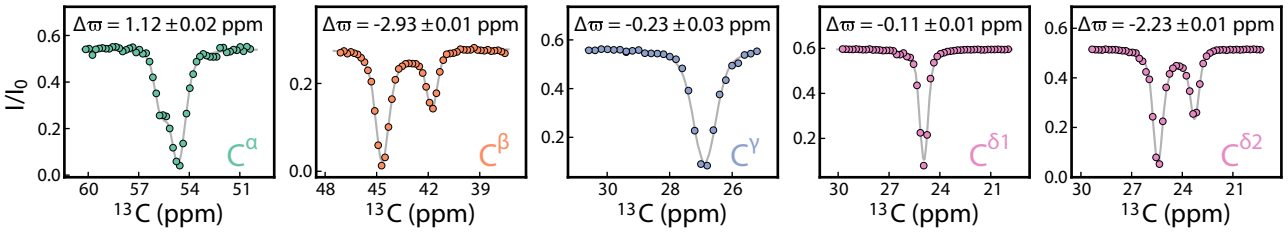

S19

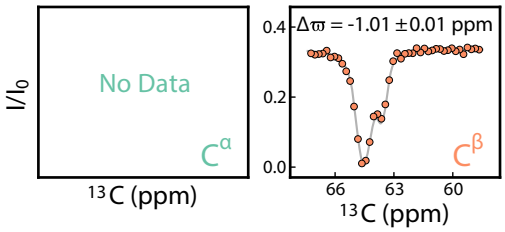

F20

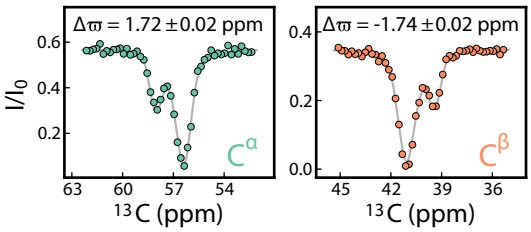

H21

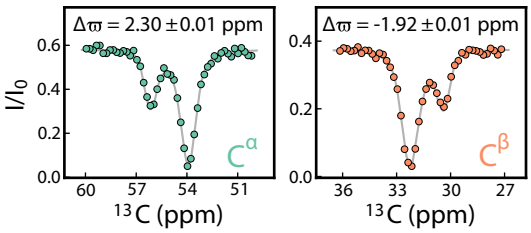

K22

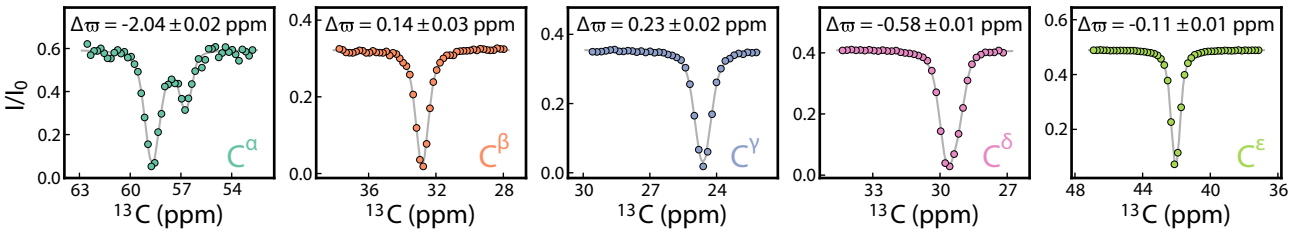

G23

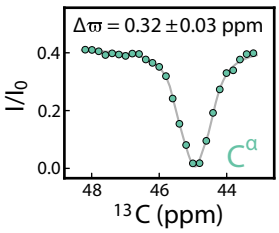

E24

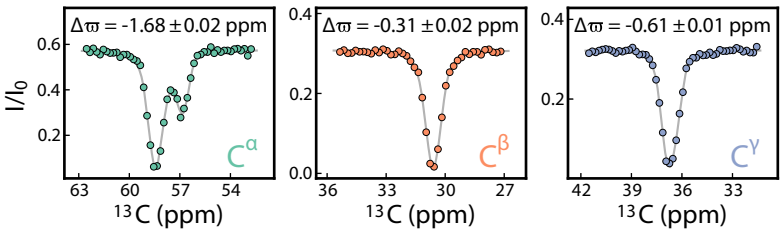

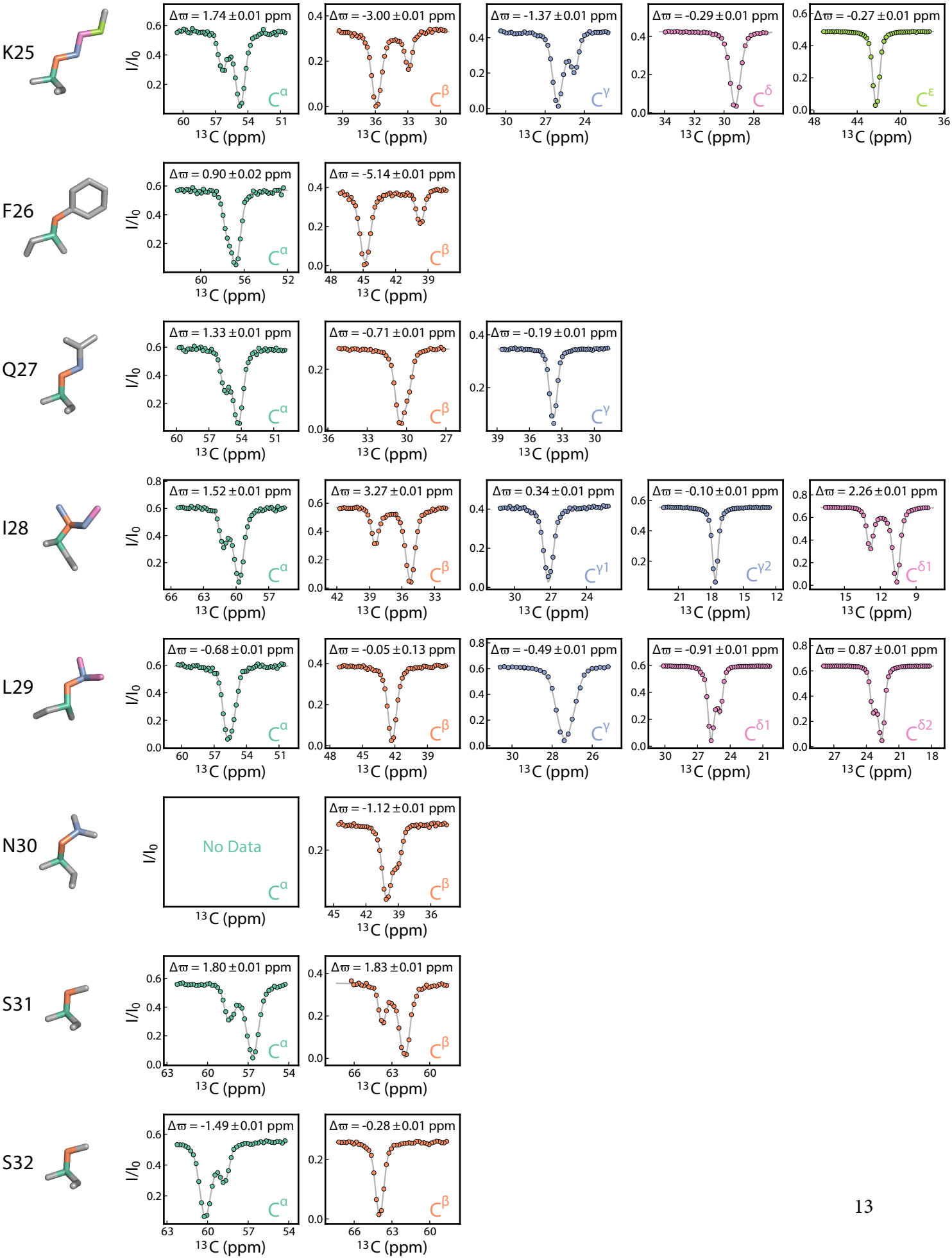
K25
Δϖ = 1.74 ±0.01 ppm
Δϖ = -3.00 ±0.01 ppm
Δϖ = -1.37 ±0.01 ppm
Δϖ = -0.29 ±0.01 ppm
Δϖ = -0.27 ±0.01 ppm
F26
Δϖ = 0.90 ±0.02 ppm
Δϖ = -5.14 ±0.01 ppm
Q27
Δϖ = 1.33 ±0.01 ppm
Δϖ = -0.71 ±0.01 ppm
Δϖ = -0.19 ±0.01 ppm
I28
Δϖ = 1.52 ±0.01 ppm
Δϖ = 3.27 ±0.01 ppm
Δϖ = 0.34 ±0.01 ppm
Δϖ = -0.10 ±0.01 ppm
Δϖ = 2.26 ±0.01 ppm
L29
Δϖ = -0.68 ±0.01 ppm
Δϖ = -0.05 ±0.13 ppm
Δϖ = -0.49 ±0.01 ppm
Δϖ = -0.91 ±0.01 ppm
Δϖ = 0.87 ±0.01 ppm
N30
No Data
Δϖ = -1.12 ±0.01 ppm
S31
Δϖ = 1.80 ±0.01 ppm
Δϖ = 1.83 ±0.01 ppm
S32
Δϖ = -1.49 ±0.01 ppm
Δϖ = -0.28 ±0.01 ppm
I/I0
13C (ppm)

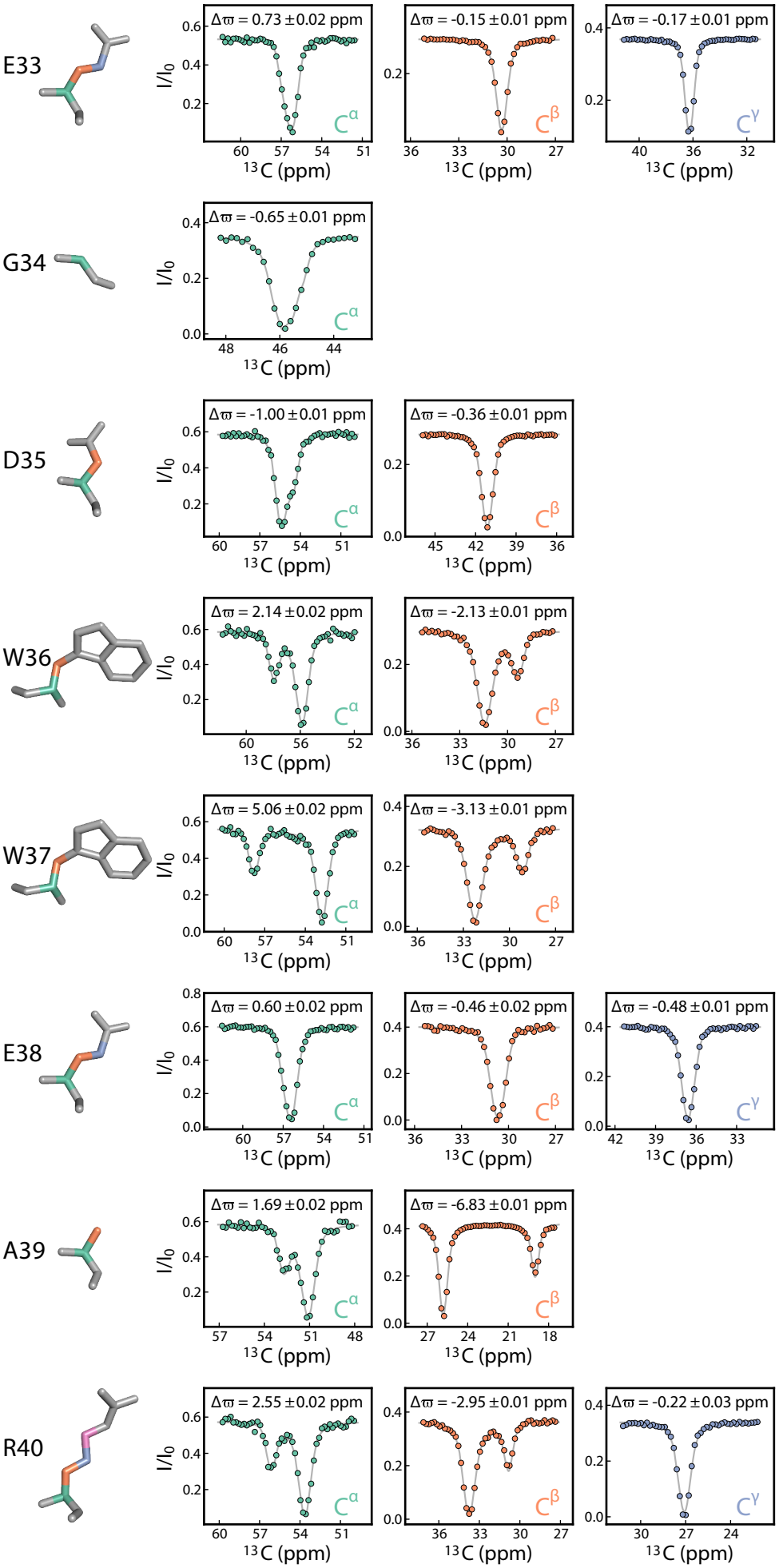
E33
Δϖ = 0.73 ±0.02 ppm
Δϖ = -0.15 ±0.01 ppm
Δϖ = -0.17 ±0.01 ppm
G34
Δϖ = -0.65 ±0.01 ppm
D35
Δϖ = -1.00 ±0.01 ppm
Δϖ = -0.36 ±0.01 ppm
W36
Δϖ = 2.14 ±0.02 ppm
Δϖ = -2.13 ±0.01 ppm
W37
Δϖ = 5.06 ±0.02 ppm
Δϖ = -3.13 ±0.01 ppm
E38
Δϖ = 0.60 ±0.02 ppm
Δϖ = -0.46 ±0.02 ppm
Δϖ = -0.48 ±0.01 ppm
A39
Δϖ = 1.69 ±0.02 ppm
Δϖ = -6.83 ±0.01 ppm
R40
Δϖ = 2.55 ±0.02 ppm
Δϖ = -2.95 ±0.01 ppm
Δϖ = -0.22 ±0.03 ppm
Δϖ = -0.22 ±0.01 ppm
I/I0
13C (ppm)

S41

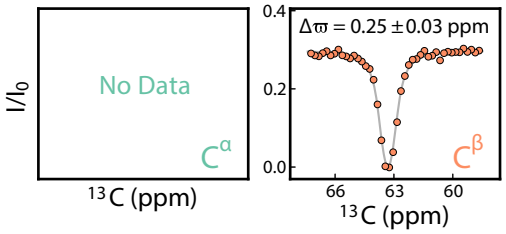

L42

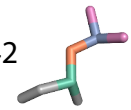

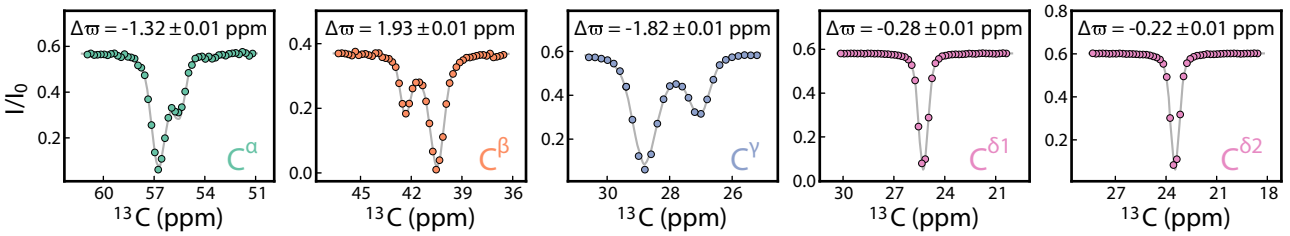

T43

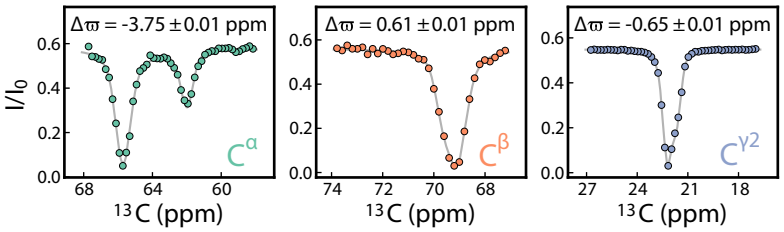

T44

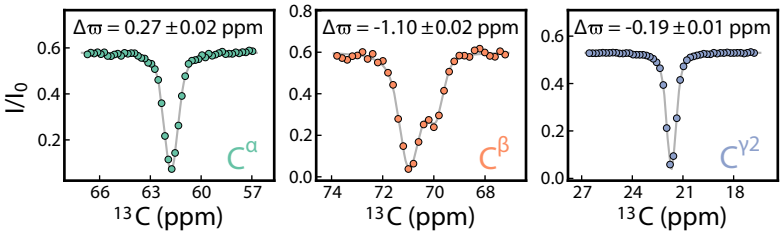

G45

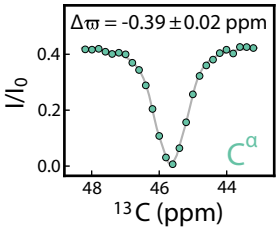

E46

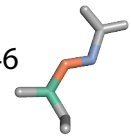

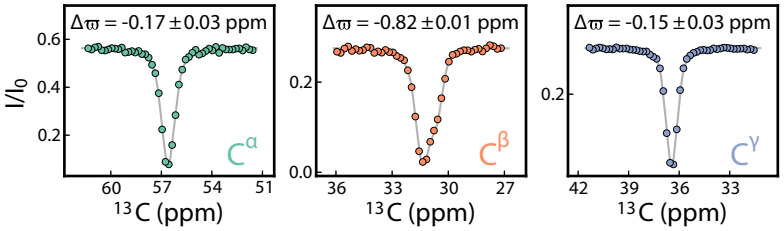

T47

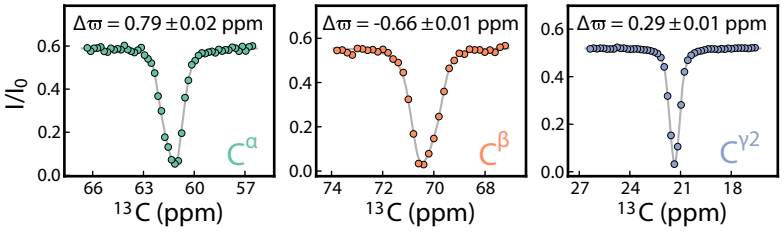

A48

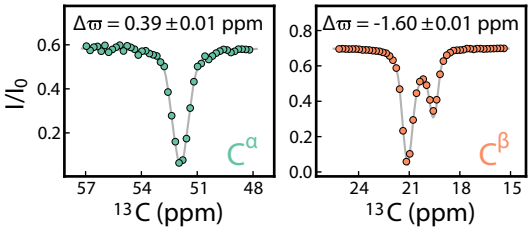

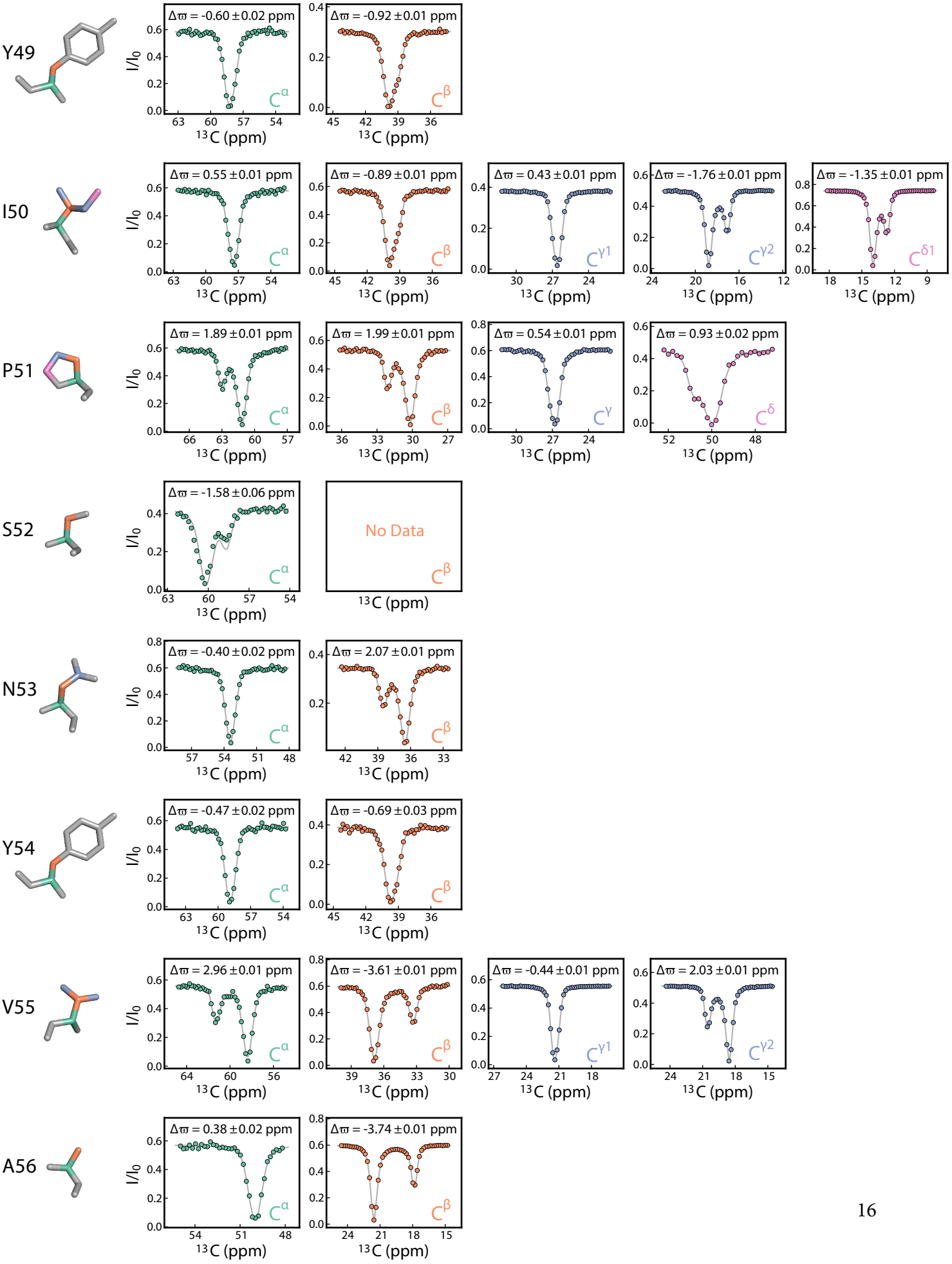
Y49
Δϖ = -0.60 ±0.02 ppm
Δϖ = -0.92 ±0.01 ppm
I50
Δϖ = 0.55 ±0.01 ppm
Δϖ = -0.89 ±0.01 ppm
Δϖ = 0.43 ±0.01 ppm
Δϖ = -1.76 ±0.01 ppm
Δϖ = -1.35 ±0.01 ppm
P51
Δϖ = 1.89 ±0.01 ppm
Δϖ = 1.99 ±0.01 ppm
Δϖ = 0.54 ±0.01 ppm
Δϖ = 0.93 ±0.02 ppm
S52
Δϖ = -1.58 ±0.06 ppm
No Data
N53
Δϖ = -0.40 ±0.02 ppm
Δϖ = 2.07 ±0.01 ppm
Y54
Δϖ = -0.47 ±0.02 ppm
Δϖ = -0.69 ±0.03 ppm
V55
Δϖ = 2.96 ±0.01 ppm
Δϖ = -3.61 ±0.01 ppm
Δϖ = -0.44 ±0.01 ppm
Δϖ = 2.03 ±0.01 ppm
A56
Δϖ = 0.38 ±0.02 ppm
Δϖ = -3.74 ±0.01 ppm
I/I0
13C (ppm)
Cα
Cβ
Cγ
Cγ1
Cγ2
Cδ
Cδ1

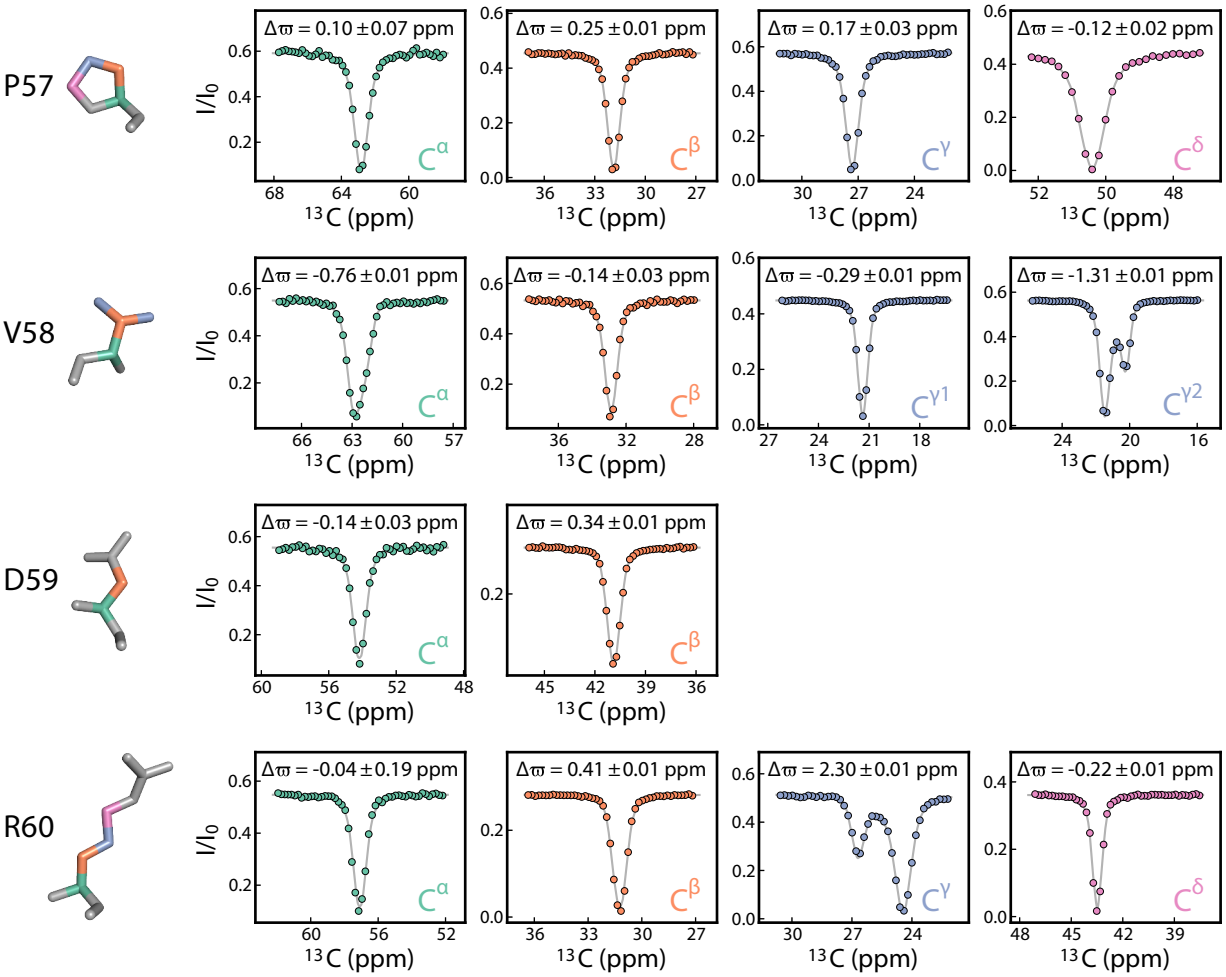
P57
Δϖ = 0.10 ±0.07 ppm
Δϖ = 0.25 ±0.01 ppm
Δϖ = 0.17 ±0.03 ppm
Δϖ = -0.12 ±0.02 ppm
V58
Δϖ = -0.76 ±0.01 ppm
Δϖ = -0.14 ±0.03 ppm
Δϖ = -0.29 ±0.01 ppm
Δϖ = -1.31 ±0.01 ppm
D59
Δϖ = -0.14 ±0.03 ppm
Δϖ = 0.34 ±0.01 ppm
R60
Δϖ = -0.04 ±0.19 ppm
Δϖ = 0.41 ±0.01 ppm
Δϖ = 2.30 ±0.01 ppm
Δϖ = -0.22 ±0.01 ppm
I/I0
13C (ppm)
Cα
Cβ
Cγ
Cγ1
Cγ2
Cδ

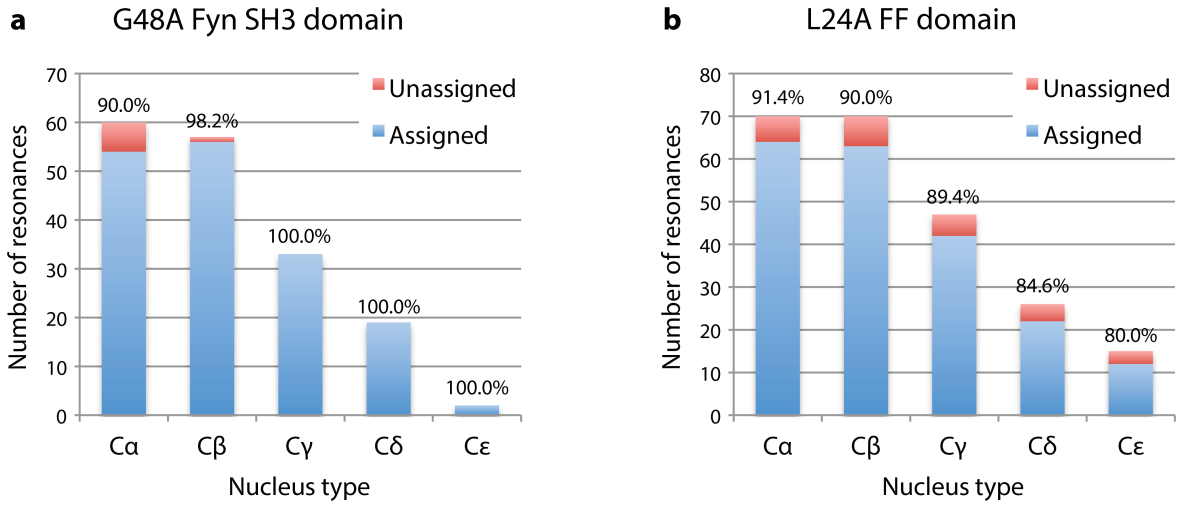

Supplementary Figure 3. Near complete aliphatic ^{13}C chemical shift assignments for the invisible, unfolded state of (a) the G48A Fyn SH3 domain and (b) a folding intermediate of the L24A FF domain. Bar graphs show the relative numbers assigned for each carbon-type.

Supplementary Figure 4. ^{13}C CEST profiles for each residue of the L24A FF domain, 25°C, 14.0T.

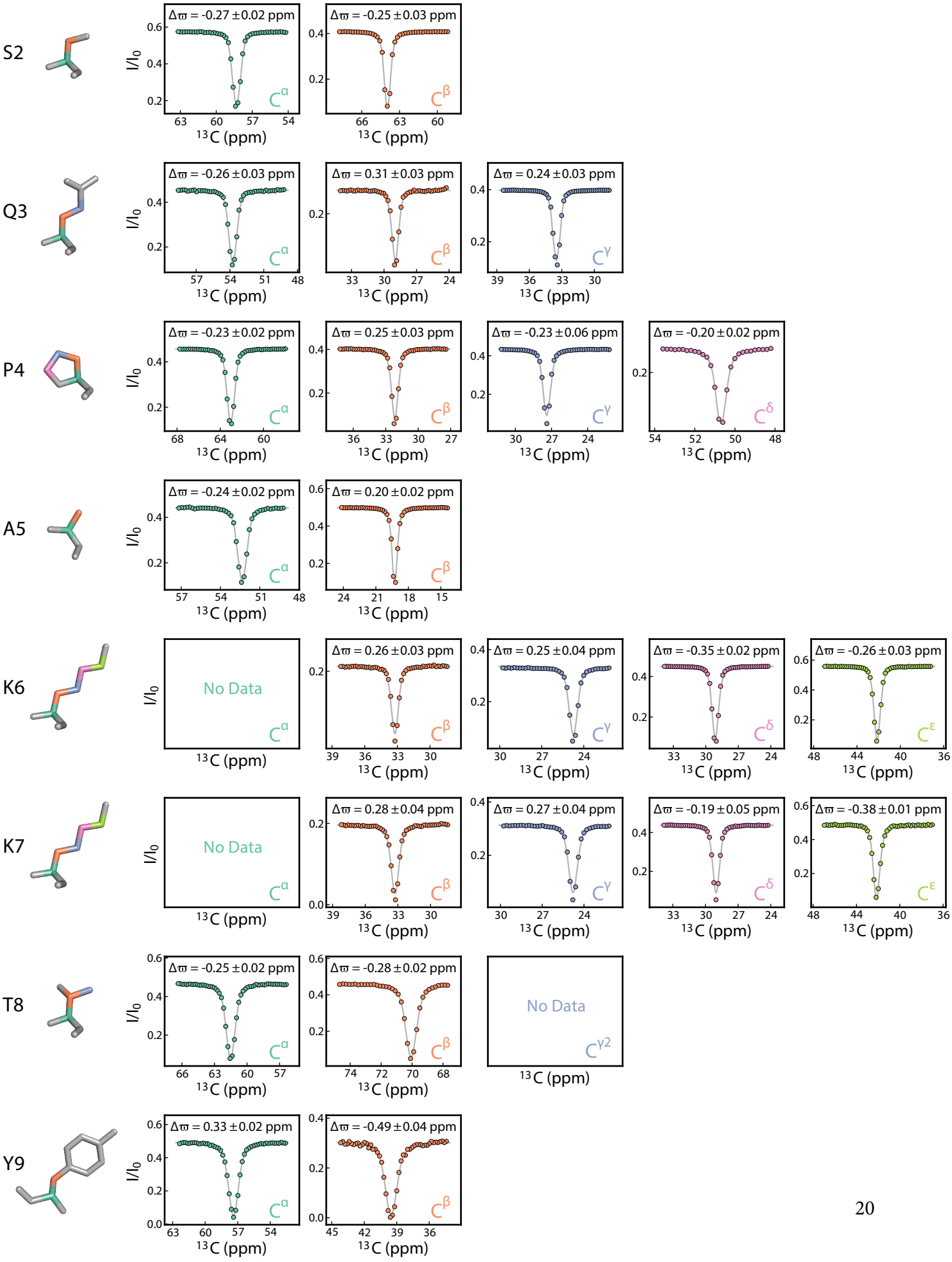
S2
Δϖ = -0.27 ±0.02 ppm
Δϖ = -0.25 ±0.03 ppm
Q3
Δϖ = -0.26 ±0.03 ppm
Δϖ = 0.31 ±0.03 ppm
Δϖ = 0.24 ±0.03 ppm
P4
Δϖ = -0.23 ±0.02 ppm
Δϖ = 0.25 ±0.03 ppm
Δϖ = -0.23 ±0.06 ppm
Δϖ = -0.20 ±0.02 ppm
A5
Δϖ = -0.24 ±0.02 ppm
Δϖ = 0.20 ±0.02 ppm
K6
No Data
Δϖ = 0.26 ±0.03 ppm
Δϖ = 0.25 ±0.04 ppm
Δϖ = -0.35 ±0.02 ppm
Δϖ = -0.26 ±0.03 ppm
K7
No Data
Δϖ = 0.28 ±0.04 ppm
Δϖ = 0.27 ±0.04 ppm
Δϖ = -0.19 ±0.05 ppm
Δϖ = -0.38 ±0.01 ppm
T8
Δϖ = -0.25 ±0.02 ppm
Δϖ = -0.28 ±0.02 ppm
No Data
Y9
Δϖ = 0.33 ±0.02 ppm
Δϖ = -0.49 ±0.04 ppm
I/I0
13C (ppm)

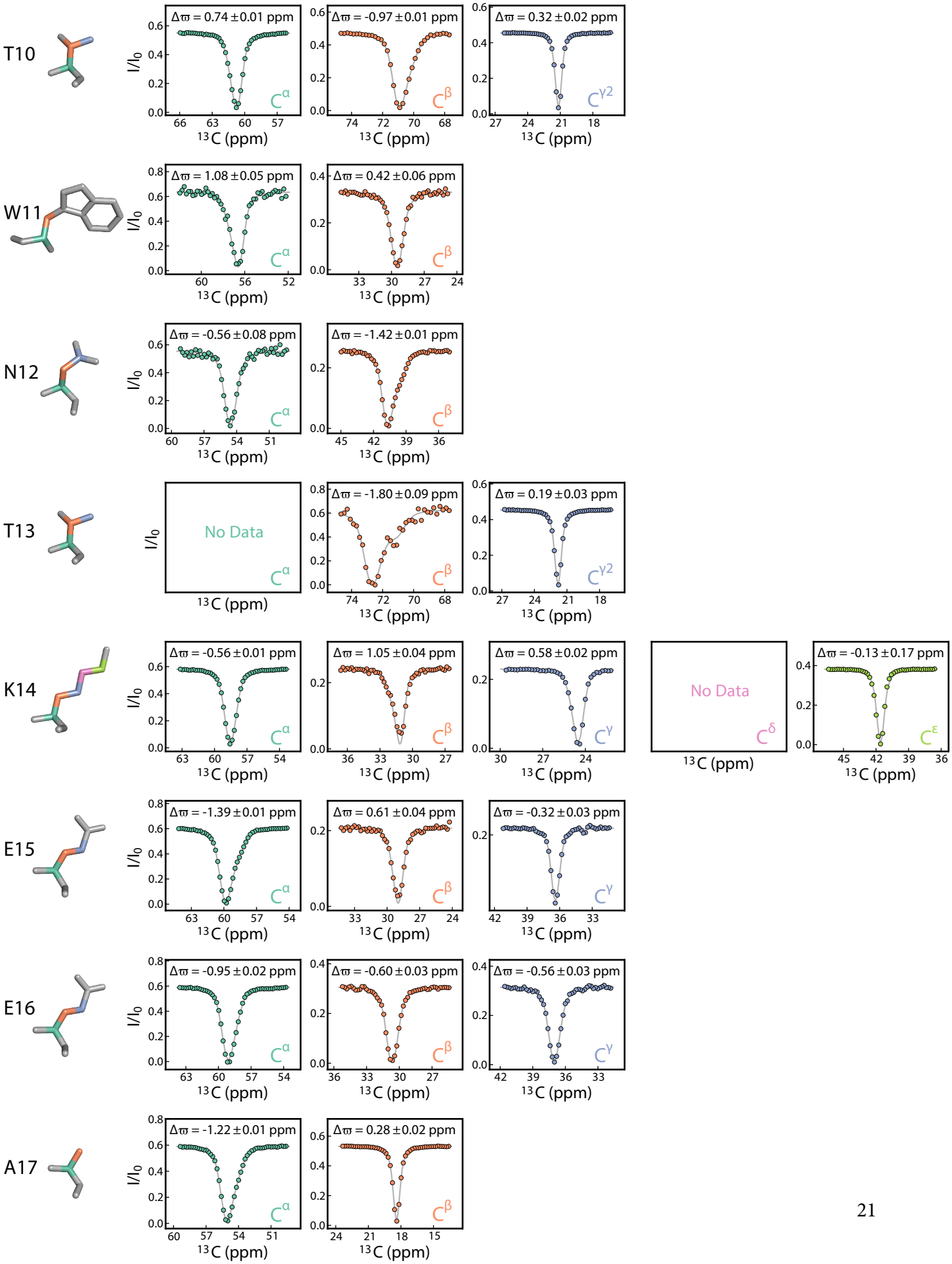
T10
Δϖ = 0.74 ±0.01 ppm
Δϖ = -0.97 ±0.01 ppm
Δϖ = 0.32 ±0.02 ppm
W11
Δϖ = 1.08 ±0.05 ppm
Δϖ = 0.42 ±0.06 ppm
N12
Δϖ = -0.56 ±0.08 ppm
Δϖ = -1.42 ±0.01 ppm
T13
No Data
Δϖ = -1.80 ±0.09 ppm
Δϖ = 0.19 ±0.03 ppm
K14
Δϖ = -0.56 ±0.01 ppm
Δϖ = 1.05 ±0.04 ppm
Δϖ = 0.58 ±0.02 ppm
No Data
Δϖ = -0.13 ±0.17 ppm
E15
Δϖ = -1.39 ±0.01 ppm
Δϖ = 0.61 ±0.04 ppm
Δϖ = -0.32 ±0.03 ppm
E16
Δϖ = -0.95 ±0.02 ppm
Δϖ = -0.60 ±0.03 ppm
Δϖ = -0.56 ±0.03 ppm
A17
Δϖ = -1.22 ±0.01 ppm
Δϖ = 0.28 ±0.02 ppm
I/I0
13C (ppm)
Cα
Cβ
Cγ2
Cγ
Cδ
Cε

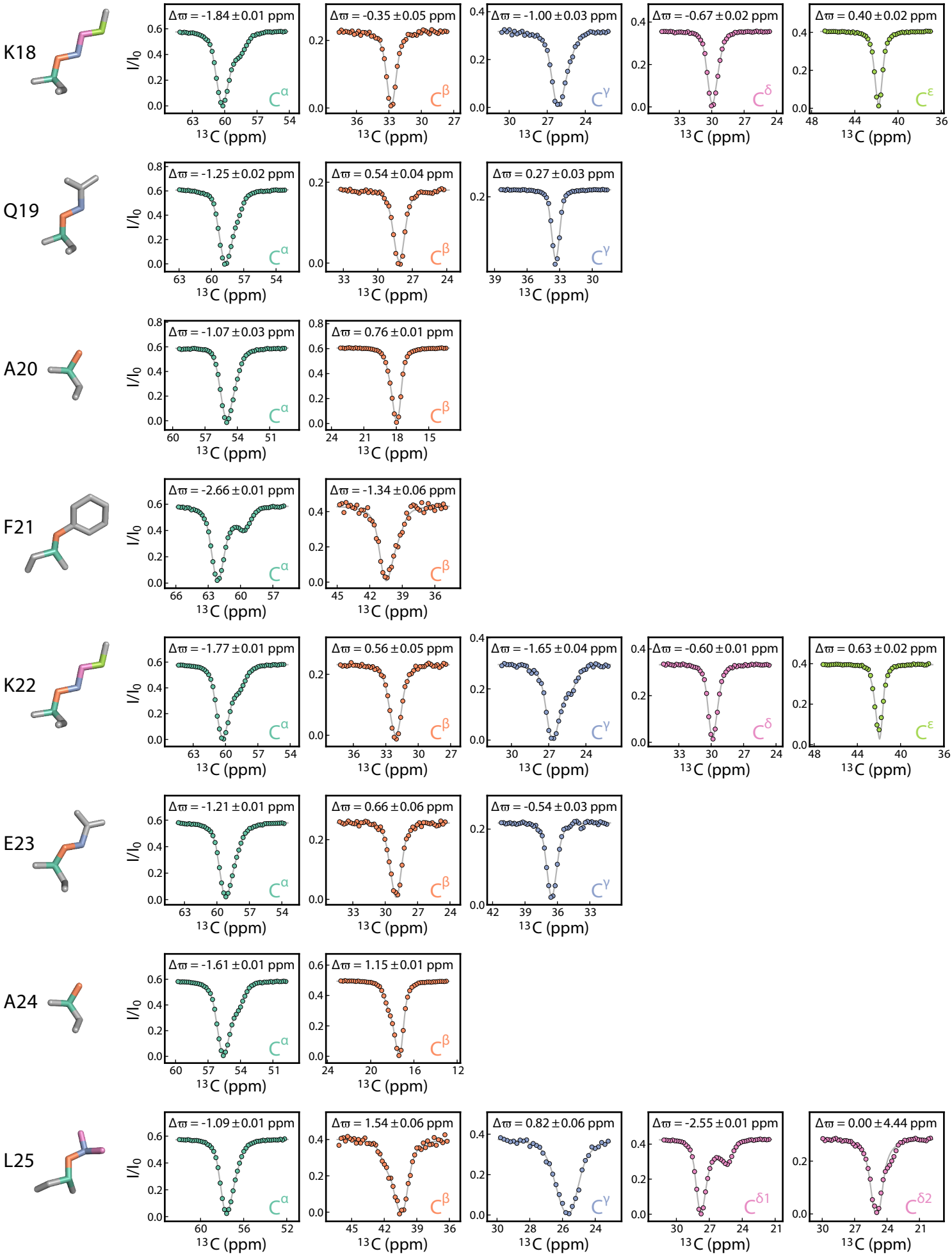
K18
Δϖ = -1.84 ±0.01 ppm
Δϖ = -0.35 ±0.05 ppm
Δϖ = -1.00 ±0.03 ppm
Δϖ = -0.67 ±0.02 ppm
Δϖ = 0.40 ±0.02 ppm
Q19
Δϖ = -1.25 ±0.02 ppm
Δϖ = 0.54 ±0.04 ppm
Δϖ = 0.27 ±0.03 ppm
A20
Δϖ = -1.07 ±0.03 ppm
Δϖ = 0.76 ±0.01 ppm
F21
Δϖ = -2.66 ±0.01 ppm
Δϖ = -1.34 ±0.06 ppm
K22
Δϖ = -1.77 ±0.01 ppm
Δϖ = 0.56 ±0.05 ppm
Δϖ = -1.65 ±0.04 ppm
Δϖ = -0.60 ±0.01 ppm
Δϖ = 0.63 ±0.02 ppm
E23
Δϖ = -1.21 ±0.01 ppm
Δϖ = 0.66 ±0.06 ppm
Δϖ = -0.54 ±0.03 ppm
A24
Δϖ = -1.61 ±0.01 ppm
Δϖ = 1.15 ±0.01 ppm
L25
Δϖ = -1.09 ±0.01 ppm
Δϖ = 1.54 ±0.06 ppm
Δϖ = 0.82 ±0.06 ppm
Δϖ = -2.55 ±0.01 ppm
Δϖ = 0.00 ±4.44 ppm
I/I0
13C (ppm)
Cα
Cβ
Cγ
Cδ
Cε
Cδ1
Cδ2

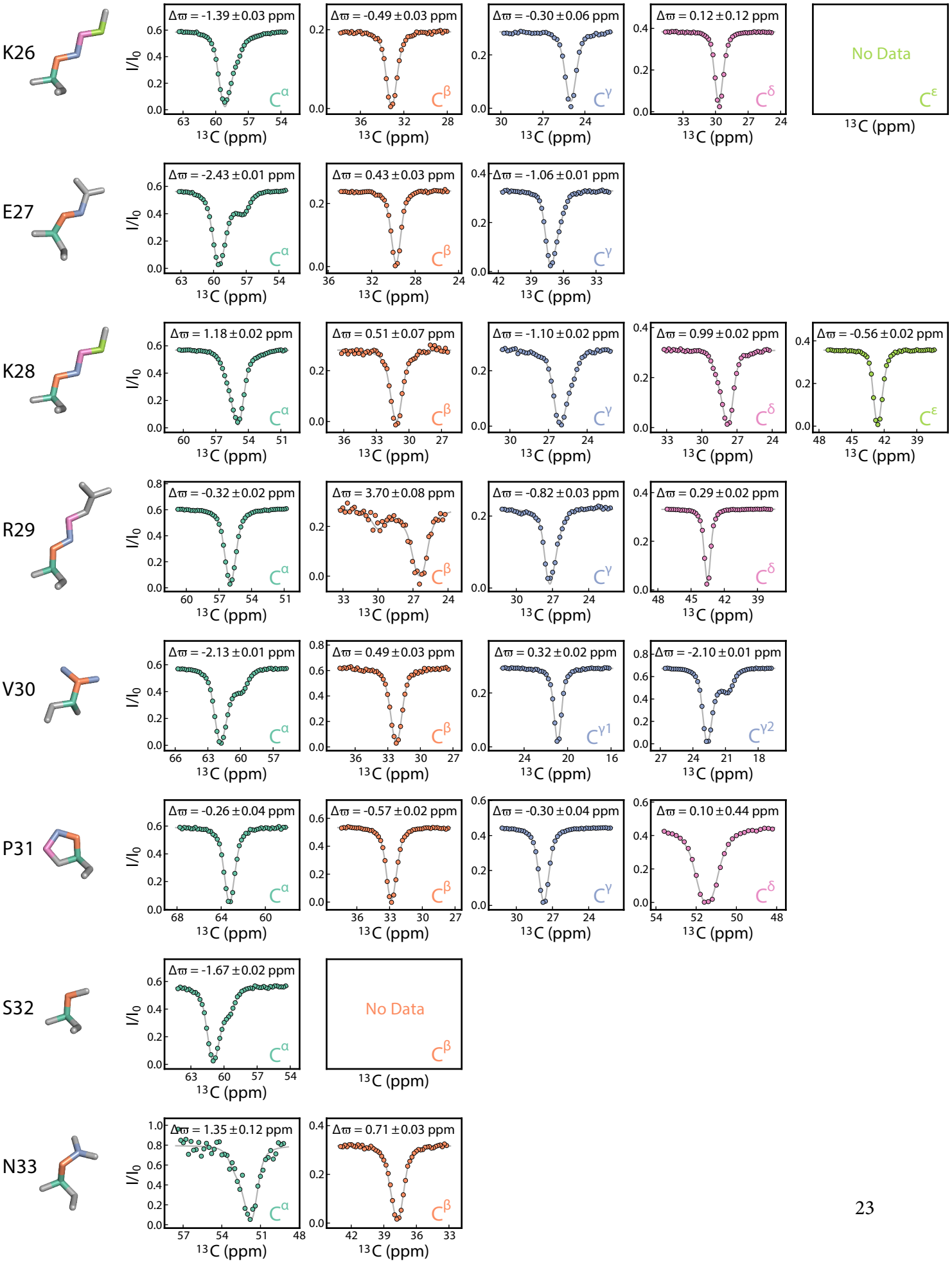
K26
Δϖ = -1.39 ± 0.03 ppm
Δϖ = -0.49 ± 0.03 ppm
Δϖ = -0.30 ± 0.06 ppm
Δϖ = 0.12 ± 0.12 ppm
No Data
E27
Δϖ = -2.43 ± 0.01 ppm
Δϖ = 0.43 ± 0.03 ppm
Δϖ = -1.06 ± 0.01 ppm
K28
Δϖ = 1.18 ± 0.02 ppm
Δϖ = 0.51 ± 0.07 ppm
Δϖ = -1.10 ± 0.02 ppm
Δϖ = 0.99 ± 0.02 ppm
Δϖ = -0.56 ± 0.02 ppm
R29
Δϖ = -0.32 ± 0.02 ppm
Δϖ = 3.70 ± 0.08 ppm
Δϖ = -0.82 ± 0.03 ppm
Δϖ = 0.29 ± 0.02 ppm
V30
Δϖ = -2.13 ± 0.01 ppm
Δϖ = 0.49 ± 0.03 ppm
Δϖ = 0.32 ± 0.02 ppm
Δϖ = -2.10 ± 0.01 ppm
P31
Δϖ = -0.26 ± 0.04 ppm
Δϖ = -0.57 ± 0.02 ppm
Δϖ = -0.30 ± 0.04 ppm
Δϖ = 0.10 ± 0.44 ppm
S32
Δϖ = -1.67 ± 0.02 ppm
No Data
N33
Δϖ = 1.35 ± 0.12 ppm
Δϖ = 0.71 ± 0.03 ppm
I/I0
13C (ppm)

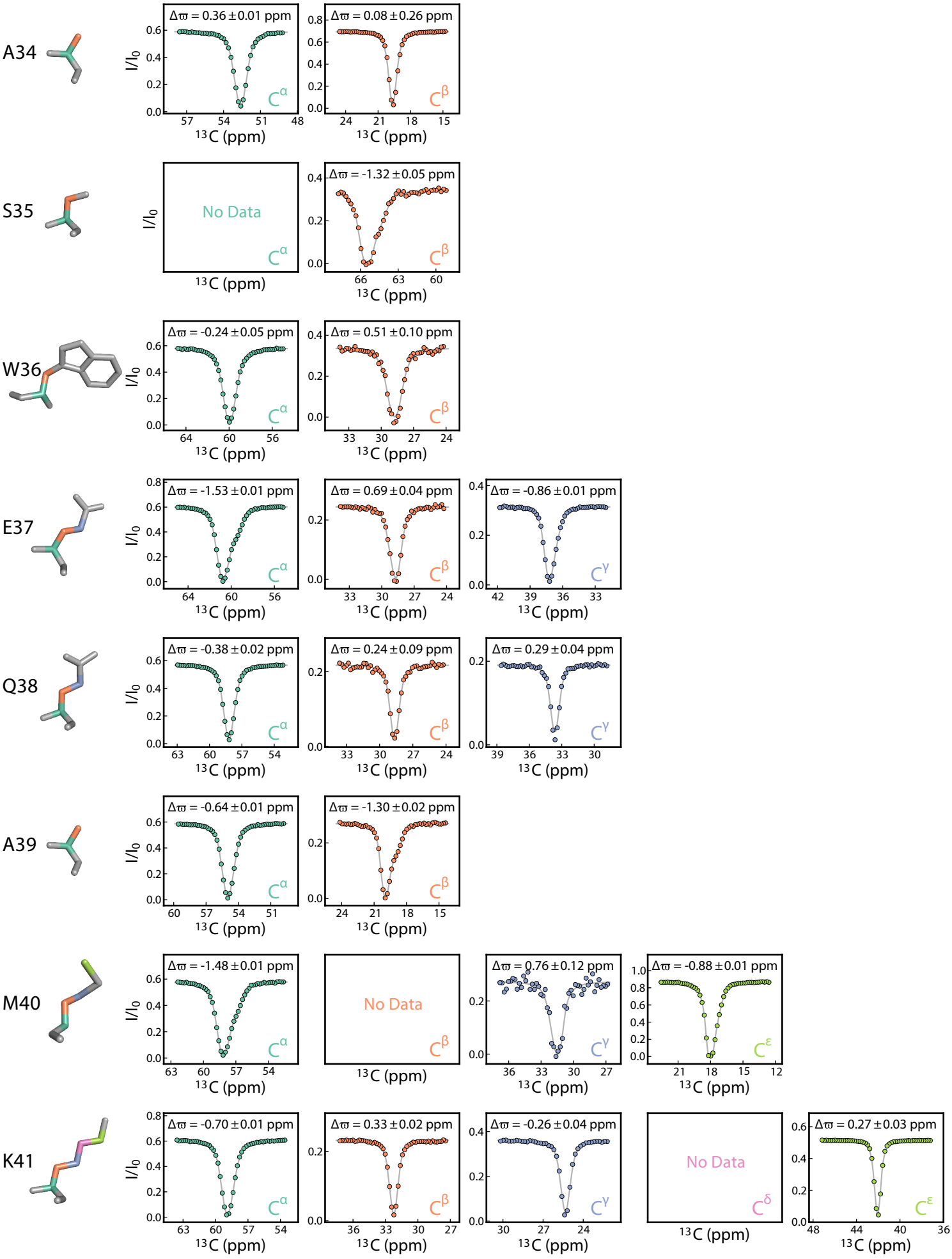
A34
Δϖ = 0.36 ±0.01 ppm
Cα
Δϖ = 0.08 ±0.26 ppm
Cβ
S35
No Data
Cα
Δϖ = -1.32 ±0.05 ppm
Cβ
W36
Δϖ = -0.24 ±0.05 ppm
Cα
Δϖ = 0.51 ±0.10 ppm
Cβ
E37
Δϖ = -1.53 ±0.01 ppm
Cα
Δϖ = 0.69 ±0.04 ppm
Cβ
Δϖ = -0.86 ±0.01 ppm
Cγ
Q38
Δϖ = -0.38 ±0.02 ppm
Cα
Δϖ = 0.24 ±0.09 ppm
Cβ
Δϖ = 0.29 ±0.04 ppm
Cγ
A39
Δϖ = -0.64 ±0.01 ppm
Cα
Δϖ = -1.30 ±0.02 ppm
Cβ
M40
Δϖ = -1.48 ±0.01 ppm
Cα
No Data
Cβ
Δϖ = 0.76 ±0.12 ppm
Cγ
Δϖ = -0.88 ±0.01 ppm
Cε
K41
Δϖ = -0.70 ±0.01 ppm
Cα
Δϖ = 0.33 ±0.02 ppm
Cβ
Δϖ = -0.26 ±0.04 ppm
Cγ
No Data
Cδ
Δϖ = 0.27 ±0.03 ppm
Cε
I/I0
13C (ppm)

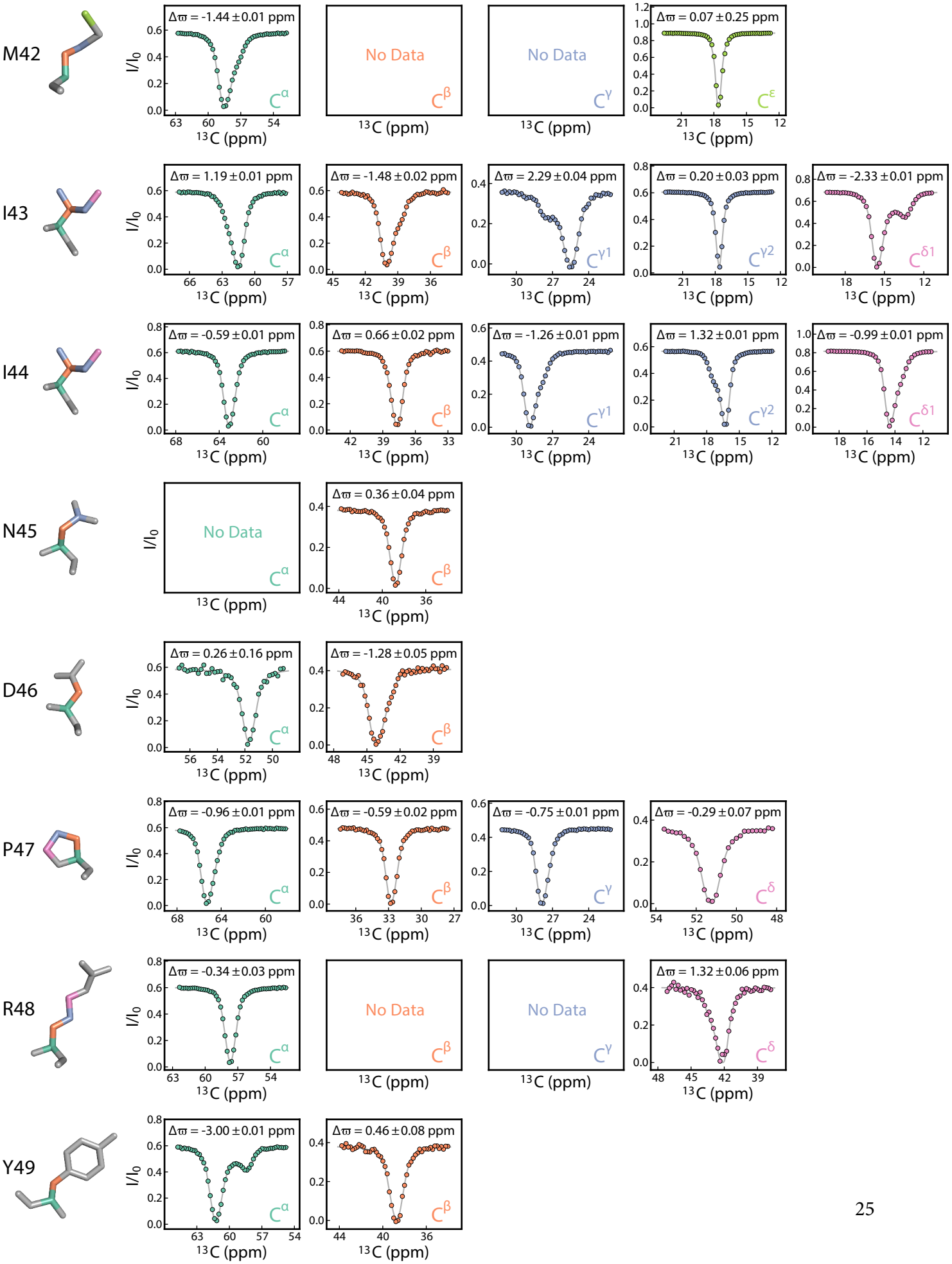
M42
Δϖ = -1.44 ±0.01 ppm
No Data
No Data
Δϖ = 0.07 ±0.25 ppm
I43
Δϖ = 1.19 ±0.01 ppm
Δϖ = -1.48 ±0.02 ppm
Δϖ = 2.29 ±0.04 ppm
Δϖ = 0.20 ±0.03 ppm
Δϖ = -2.33 ±0.01 ppm
I44
Δϖ = -0.59 ±0.01 ppm
Δϖ = 0.66 ±0.02 ppm
Δϖ = -1.26 ±0.01 ppm
Δϖ = 1.32 ±0.01 ppm
Δϖ = -0.99 ±0.01 ppm
N45
No Data
Δϖ = 0.36 ±0.04 ppm
D46
Δϖ = 0.26 ±0.16 ppm
Δϖ = -1.28 ±0.05 ppm
P47
Δϖ = -0.96 ±0.01 ppm
Δϖ = -0.59 ±0.02 ppm
Δϖ = -0.75 ±0.01 ppm
Δϖ = -0.29 ±0.07 ppm
R48
Δϖ = -0.34 ±0.03 ppm
No Data
No Data
Δϖ = 1.32 ±0.06 ppm
Y49
Δϖ = -3.00 ±0.01 ppm
Δϖ = 0.46 ±0.08 ppm
I/I0
13C (ppm)

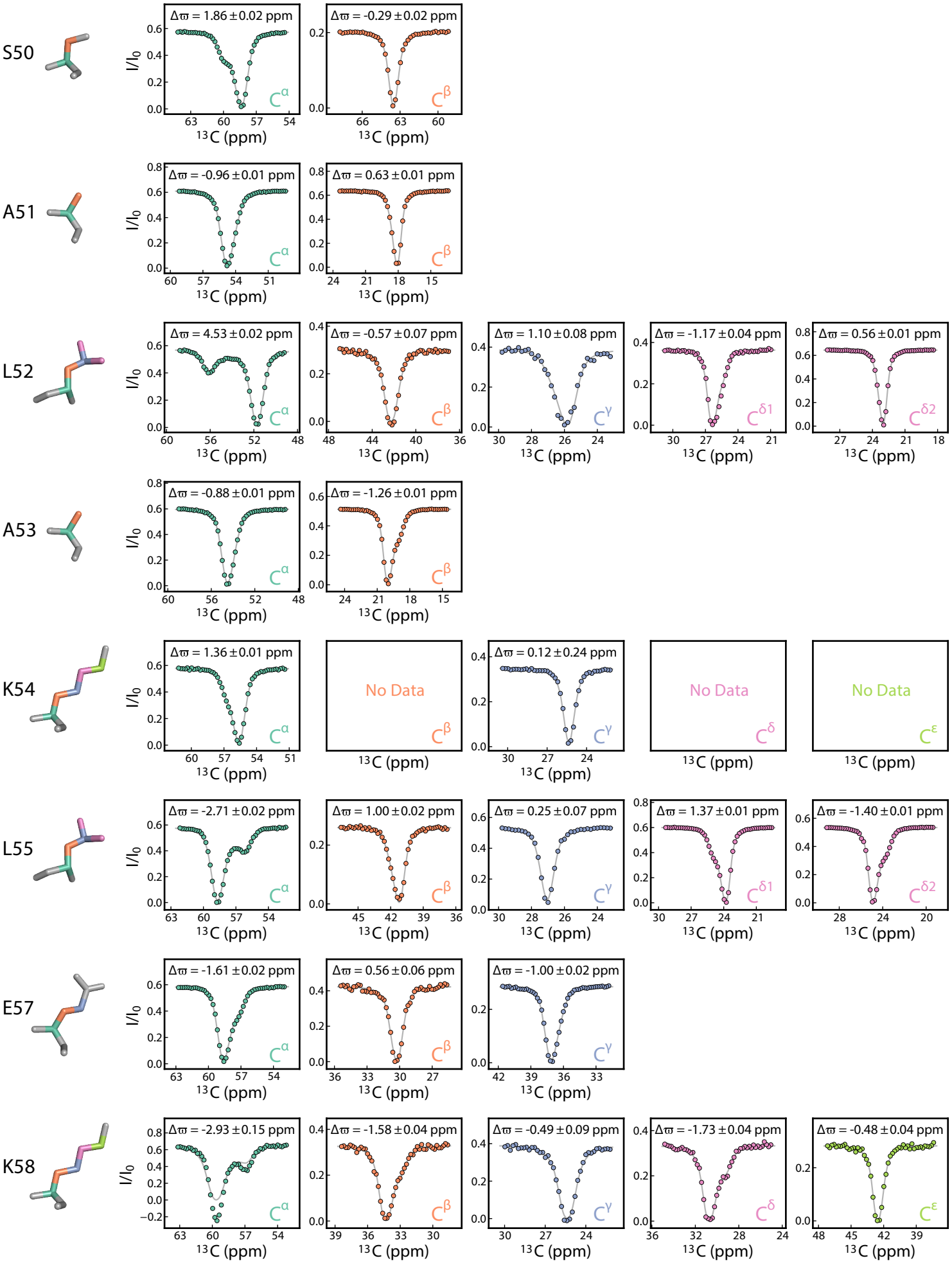
S50
Δϖ = 1.86 ±0.02 ppm
Δϖ = -0.29 ±0.02 ppm
A51
Δϖ = -0.96 ±0.01 ppm
Δϖ = 0.63 ±0.01 ppm
L52
Δϖ = 4.53 ±0.02 ppm
Δϖ = -0.57 ±0.07 ppm
Δϖ = 1.10 ±0.08 ppm
Δϖ = -1.17 ±0.04 ppm
Δϖ = 0.56 ±0.01 ppm
A53
Δϖ = -0.88 ±0.01 ppm
Δϖ = -1.26 ±0.01 ppm
K54
Δϖ = 1.36 ±0.01 ppm
No Data
Δϖ = 0.12 ±0.24 ppm
No Data
No Data
L55
Δϖ = -2.71 ±0.02 ppm
Δϖ = 1.00 ±0.02 ppm
Δϖ = 0.25 ±0.07 ppm
Δϖ = 1.37 ±0.01 ppm
Δϖ = -1.40 ±0.01 ppm
E57
Δϖ = -1.61 ±0.02 ppm
Δϖ = 0.56 ±0.06 ppm
Δϖ = -1.00 ±0.02 ppm
K58
Δϖ = -2.93 ±0.15 ppm
Δϖ = -1.58 ±0.04 ppm
Δϖ = -0.49 ±0.09 ppm
Δϖ = -1.73 ±0.04 ppm
Δϖ = -0.48 ±0.04 ppm
I/I0
13C (ppm)

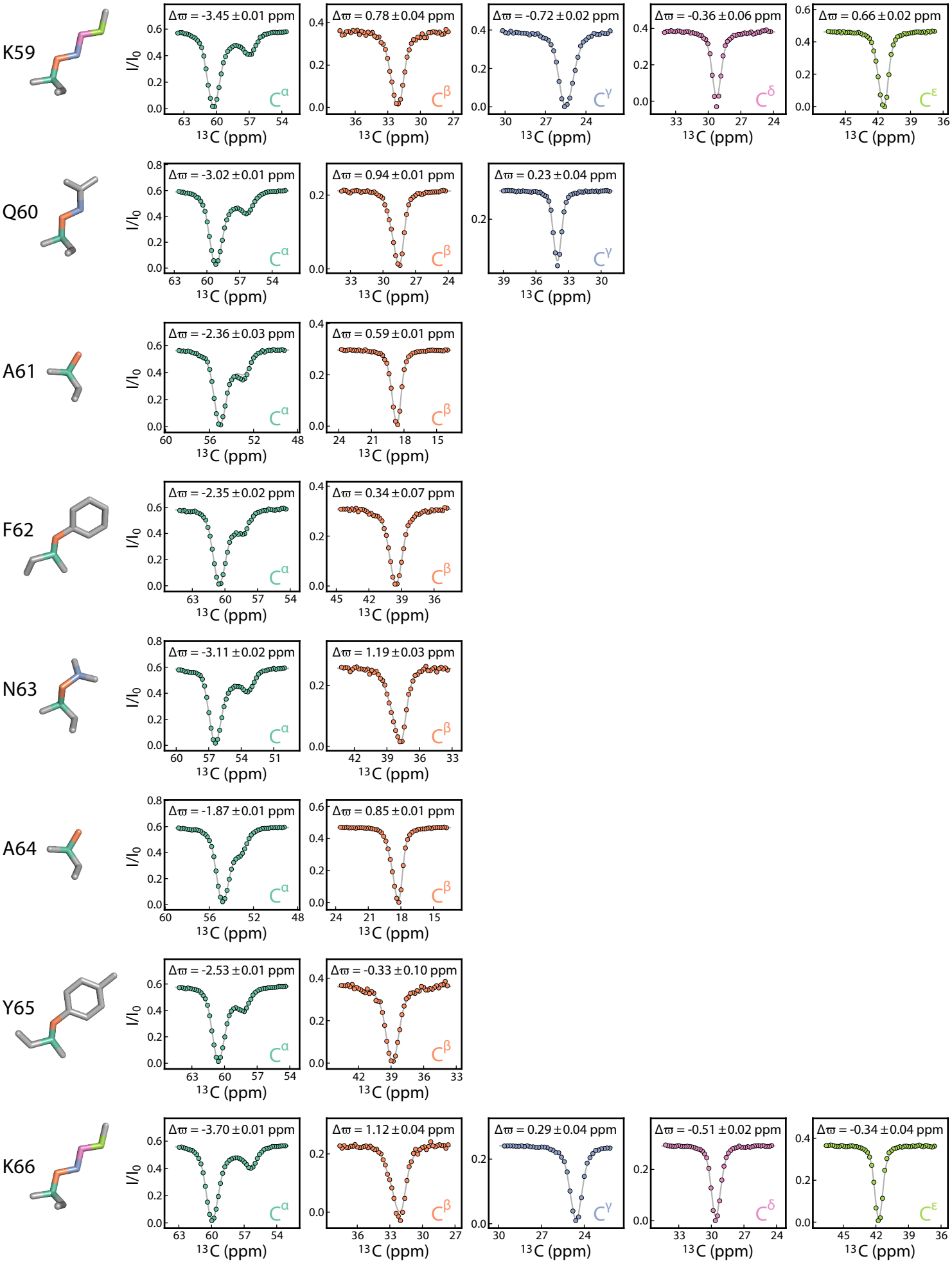
K59
Δϖ = -3.45 ±0.01 ppm
Δϖ = 0.78 ±0.04 ppm
Δϖ = -0.72 ±0.02 ppm
Δϖ = -0.36 ±0.06 ppm
Δϖ = 0.66 ±0.02 ppm
Q60
Δϖ = -3.02 ±0.01 ppm
Δϖ = 0.94 ±0.01 ppm
Δϖ = 0.23 ±0.04 ppm
A61
Δϖ = -2.36 ±0.03 ppm
Δϖ = 0.59 ±0.01 ppm
F62
Δϖ = -2.35 ±0.02 ppm
Δϖ = 0.34 ±0.07 ppm
N63
Δϖ = -3.11 ±0.02 ppm
Δϖ = 1.19 ±0.03 ppm
A64
Δϖ = -1.87 ±0.01 ppm
Δϖ = 0.85 ±0.01 ppm
Y65
Δϖ = -2.53 ±0.01 ppm
Δϖ = -0.33 ±0.10 ppm
K66
Δϖ = -3.70 ±0.01 ppm
Δϖ = 1.12 ±0.04 ppm
Δϖ = 0.29 ±0.04 ppm
Δϖ = -0.51 ±0.02 ppm
Δϖ = -0.34 ±0.04 ppm
I/I0
13C (ppm)
Cα
Cβ
Cγ
Cδ
Cε

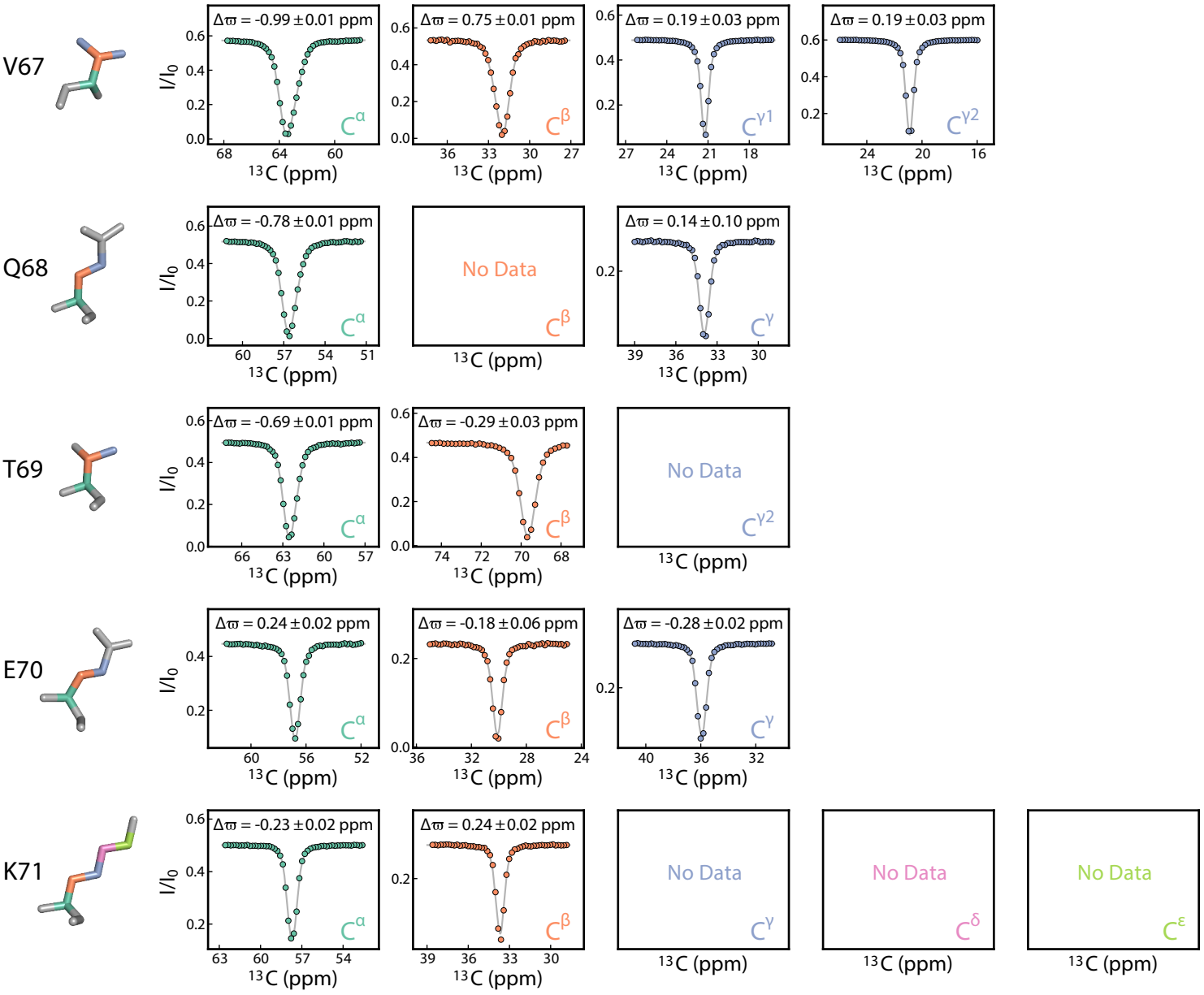
V67
Δϖ = -0.99 ±0.01 ppm
Cα
Δϖ = 0.75 ±0.01 ppm
Cβ
Δϖ = 0.19 ±0.03 ppm
Cγ1
Δϖ = 0.19 ±0.03 ppm
Cγ2
Q68
Δϖ = -0.78 ±0.01 ppm
Cα
No Data
Cβ
Δϖ = 0.14 ±0.10 ppm
Cγ
T69
Δϖ = -0.69 ±0.01 ppm
Cα
Δϖ = -0.29 ±0.03 ppm
Cβ
No Data
Cγ2
E70
Δϖ = 0.24 ±0.02 ppm
Cα
Δϖ = -0.18 ±0.06 ppm
Cβ
Δϖ = -0.28 ±0.02 ppm
Cγ
K71
Δϖ = -0.23 ±0.02 ppm
Cα
Δϖ = 0.24 ±0.02 ppm
Cβ
No Data
Cγ
No Data
Cδ
No Data
Cε
I/I0
13C (ppm)

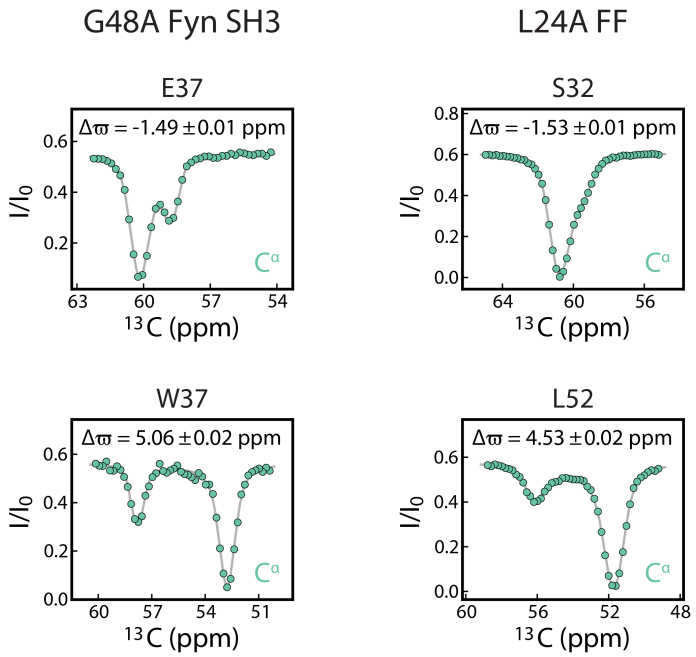

Supplementary Figure 5. Resolution in CEST profiles decreases with increasing k_{ex}. Comparison of selected CEST profiles recorded at 14.0T, 25°C for the G48A Fyn SH3 (k_{ex} ~ 130 s^{-1}) and the L24A FF (k_{ex} ~ 540 s^{-1}) domains. The top and bottom pair of profiles derive from ^{13}C nuclei with similar $\Delta\varpi$ values. The differences in resolution between major and minor state dips (compare traces in top or traces in bottom) reflect the differences in linewidths of the minor state peaks that in turn results in large part from differences in exchange rates.

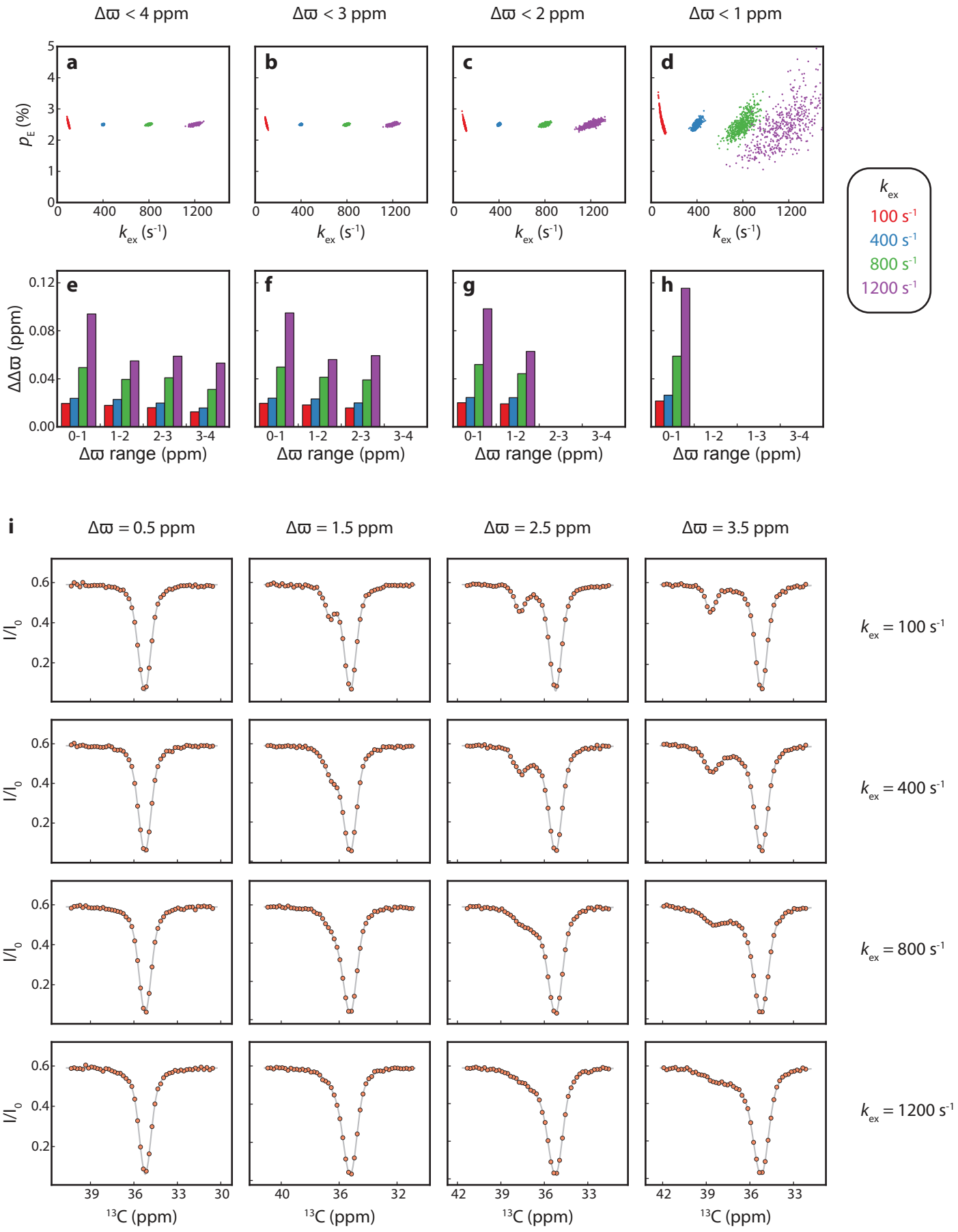
Δϖ < 4 ppm
Δϖ < 3 ppm
Δϖ < 2 ppm
Δϖ < 1 ppm
a
b
c
d
p_E (%)
k_{ex} (s^{-1})
k_{ex}
100 s^{-1}
400 s^{-1}
800 s^{-1}
1200 s^{-1}
e
f
g
h
ΔΔϖ (ppm)
Δϖ range (ppm)
0-1
1-2
2-3
3-4
1-3
i
Δϖ = 0.5 ppm
Δϖ = 1.5 ppm
Δϖ = 2.5 ppm
Δϖ = 3.5 ppm
I/I_0
k_{ex} = 100 s^{-1}
k_{ex} = 400 s^{-1}
k_{ex} = 800 s^{-1}
k_{ex} = 1200 s^{-1}
^{13}C (ppm)

Supplementary Figure 6. Robustness of extracted chemical exchange parameters and $\Delta\varpi$ values as a function of k_{ex}. Data sets were simulated based on extracted ^{13}C R_1, R_2 and shift difference values from a subset of residues of Fyn SH3 as described in detail under the section "Simulations to establish the robustness of CEST data". Simulated CEST profiles with input p_E = 2.5% and k_{ex} = {100 s^{-1}, 400 s^{-1}, 800 s^{-1}, 1200 s^{-1}} were generated following a Monte Carlo procedure[20] and then fit to produce the p_E, k_{ex} distributions in a-d for input values of k_{ex} = 100 s^{-1} (red), 400 s^{-1} (blue), 800 s^{-1} (green), 1200 s^{-1} (purple). Errors in extracted $\Delta\varpi$ values, $\Delta\Delta\varpi$, for each value of k_{ex} are given in the bar graphs in e-h (color coded as for a-d). Values of $\Delta\varpi$ are separated into 4 classes, including $\Delta\varpi$ < 1 ppm, 1ppm-2ppm, 2ppm-3ppm, 3ppm-4ppm for each of the input k_{ex} values. Simulations were carried out for all residues (a,e), those for which $\Delta\varpi \leq$ 3ppm (b,f), $\Delta\varpi \leq$ 2ppm (c,g) and $\Delta\varpi \leq$ 1ppm (d,h). (i) Simulated CEST profiles for a single ^{13}C spin (corresponding to $I28C^{\beta}$ of the Fyn SH3 domain) as a function of k_{ex} and $\Delta\varpi$. Values of p_E = 2.5%, ^{13}C R_1= 18.6 s^{-1}, ^{13}C R_2= 2.2 s^{-1} were used in the simulations.

Supplementary Table 1. Experimental details

Type[a]	CEST range[b] (ppm)	Number of Planes[c]	Complex t_1-points[d]	Time[e] (h)	^{13}C dec[f] (ppm)	^{15}N dec[g] (ppm)
a CT-CH_3	[8.0;31.1] *All CH_3 groups*	117	55	27	–	–
a CT-CH_2	[22.2;31.2] *[R,K,P]-γ, I-γ1*	46	69	13½	–	–
	[27.2;47.1] *[C,D,E,F,H,I,K,L,M,N, P,Q,R,V,W,Y]-β, [E,M,Q]-γ, [K,R]-δ, K-ε*	101	66	28	[-118;-28] [190;100]	[30;40] [80;90]
	[47.2;52.2] *P-δ*	26	66	7½	–	[120;145]
	[58.6;67.2] *S-β*	44	66	12¼	–	–
a nCT-CH_2	[43.2;48.2] *G-α*	26	66	7¼	–	[100;140]
a CT-CH	[25.2;30.6] *L-γ*	28	66	7¾	–	–
	[67.0;73.6] *T-β*	34	66	9½	–	–
a nCT-CH	[58.4;65.6] *S-α*	44	48	8¼	[165;185]	[100;140]
b	[48.2;67.7] *All α but [G,S]-α*	99	66	27½	[16;46] [100;70] [168;182]	–

[a]The type of experiment used (*ie*, Supplementary Fig. 1a CT-t_1, 1a nCT-t_1, or 1b) as well as the type of spin system (CH_3, CH_2 or CH) is listed.

[b]^{13}C chemical shift range over which the weak B_1 field is applied, along with a list of the carbons (residue and position) that are affected. Values are for the Fyn SH3 domain application, with

similar values used for the FF domain. For example [8.0;31.1] means that planes are recorded with the position of the CEST field ranging from 8.0 ppm to 31.1 ppm (one frequency per plane).

[c]Number of planes, where each plane corresponds to a particular position of the CEST B_1 field extending from frequency a to b, listed as [a;b].

[d]Number of complex t_1 points.

[e]Time to record the complete CEST dataset.

[f]Constant adiabaticity WURST-8 decoupling schemes[8; 9] were applied over the ^{13}C chemical shift range as indicated. Case 1: [-118;-28],[190;100] indicates two fields applied simultaneously centered at -73 ppm and 145 ppm, respectively, bandwidth of 90 ppm that are swept in opposite directions to minimize Bloch-Siegert effects over the region of interest[10; 11] centered at ~ 36 ppm (CH_2). The net field has a max(rms) field strength of 2.12(1.14) kHz. Decoupling of aromatic Cγ and carbonyls is achieved. Case 2: [165;185], constant adiabaticity WURST-8 decoupling centered at 175 ppm, bandwidth of 20 ppm with a max(rms) field strength of 0.47(0.38) kHz. Decoupling of carbonyls. Case 3: [16;46],[100;70],[168;182], constant adiabaticity WURST-8 decoupling centered at 31 ppm [16;46] and 85 ppm [100;70], swept in opposite directions along with constant adiabaticity WURST-8 decoupling centered at 175 ppm [168;182]. Essentially all Cβ carbons with the exception of Cβ(Ser) are decoupled in this manner, generating $^{13}C^{\alpha}$-$^{1}H^{\alpha}$ spectra with high sensitivity and resolution. The net field has a max(rms) field strength of 1.5(0.65) kHz.

[g]WURST-2[19] decoupling schemes applied over the ^{15}N ranges (ppm) indicated to decouple ^{15}N (Lys-Nζ[30;40]; Arg-Nε[80;90];Pro-Nδ[120;145];all backbone[100;140]).

Supplementary Table 2. Ground (ϖ_G) and excited (ϖ_E) state chemical shifts of the A39G Fyn SH3 domain, 25°C.[a]

Residue	Nucleus	ϖ_G (ppm)	ϖ_E (ppm)
S1	Cα	58.11	57.78 ± 0.01
S1	Cβ	64.88	64.60 ± 0.01
T2	Cα	61.95	61.85 ± 0.04
T2	Cβ	70.03	69.85 ± 0.02
T2	Cγ2	21.86	21.67 ± 0.01
L3	Cα	54.66	55.54 ± 0.02
L3	Cβ	43.87	42.27 ± 0.01
L3	Cγ	27.11	26.88 ± 0.03
L3	Cδ1	25.09	24.71 ± 0.01
L3	Cδ2	24.26	23.65 ± 0.01
F4	Cα	56.52	57.85 ± 0.01
F4	Cβ	43.49	39.44 ± 0.01
E5	Cα	53.30	56.64 ± 0.01
E5	Cβ	34.34	30.46 ± 0.01
E5	Cγ	35.53	36.34 ± 0.01
A6	Cα	52.20	52.45 ± 0.04
A6	Cβ	20.94	19.12 ± 0.01
L7	Cα	55.64	55.24 ± 0.02
L7	Cβ	43.23	42.49 ± 0.02
L7	Cγ	26.78	26.94 ± 0.03
L7	Cδ1	25.35	24.92 ± 0.01
L7	Cδ2	21.92	23.47 ± 0.01
Y8	Cα	53.75	57.51 ± 0.01
Y8	Cβ	42.67	38.94 ± 0.01
D9	Cα	54.60	-
D9	Cβ	42.17	40.99 ± 0.01
Y10	Cα	58.02	58.47 ± 0.01
Y10	Cβ	41.85	38.64 ± 0.02
E11	Cα	53.81	56.56 ± 0.01
E11	Cβ	30.87	30.33 ± 0.01
E11	Cγ	36.10	36.43 ± 0.01
A12	Cα	52.90	52.47 ± 0.01

Residue	Nucleus	ϖ_G (ppm)	ϖ_E (ppm)
A12	Cβ	19.44	19.05 ± 0.01
R13	Cα	56.39	55.90 ± 0.01
R13	Cβ	32.62	30.99 ± 0.01
R13	Cγ	26.79	27.05 ± 0.01
R13	Cδ	43.44	43.22 ± 0.01
T14	Cα	59.68	-
T14	Cβ	71.39	69.95 ± 0.03
T14	Cγ2	21.26	21.66 ± 0.01
E15	Cα	57.64	57.14 ± 0.01
E15	Cβ	29.60	30.04 ± 0.01
E15	Cγ	36.48	36.21 ± 0.01
D16	Cα	54.30	-
D16	Cβ	42.34	41.26 ± 0.01
D17	Cα	52.64	54.70 ± 0.01
D17	Cβ	42.83	41.20 ± 0.01
L18	Cα	54.64	55.75 ± 0.02
L18	Cβ	44.68	41.75 ± 0.01
L18	Cγ	26.91	26.68 ± 0.03
L18	Cδ1	24.95	24.84 ± 0.01
L18	Cδ2	25.46	23.23 ± 0.01
S19	Cα	58.15	-
S19	Cβ	64.55	63.54 ± 0.01
F20	Cα	56.37	58.10 ± 0.02
F20	Cβ	41.09	39.35 ± 0.02
H21	Cα	53.90	56.20 ± 0.01
H21	Cβ	32.27	30.35 ± 0.01
K22	Cα	58.71	56.67 ± 0.02
K22	Cβ	32.81	32.95 ± 0.03
K22	Cγ	24.59	24.82 ± 0.02
K22	Cδ	29.69	29.11 ± 0.01
K22	Cε	42.05	41.94 ± 0.01
G23	Cα	44.90	45.22 ± 0.03
E24	Cα	58.46	56.77 ± 0.02
E24	Cβ	30.65	30.34 ± 0.02

Residue	Nucleus	ϖ_G (ppm)	ϖ_E (ppm)
E24	Cγ	36.85	36.24 ± 0.01
K25	Cα	54.68	56.42 ± 0.01
K25	Cβ	35.90	32.90 ± 0.01
K25	Cγ	26.07	24.71 ± 0.01
K25	Cδ	29.30	29.00 ± 0.01
K25	Cε	42.29	42.02 ± 0.01
F26	Cα	56.75	57.64 ± 0.02
F26	Cβ	44.83	39.69 ± 0.01
Q27	Cα	54.27	55.60 ± 0.01
Q27	Cβ	30.52	29.82 ± 0.01
Q27	Cγ	33.81	33.63 ± 0.01
I28	Cα	59.70	61.22 ± 0.01
I28	Cβ	35.21	38.48 ± 0.01
I28	Cγ1	27.11	27.44 ± 0.01
I28	Cγ2	17.60	17.50 ± 0.01
I28	Cδ1	10.63	12.89 ± 0.01
L29	Cα	55.77	55.09 ± 0.01
L29	Cβ	42.24	42.19 ± 0.13
L29	Cγ	27.45	26.97 ± 0.01
L29	Cδ1	25.79	24.87 ± 0.01
L29	Cδ2	22.57	23.44 ± 0.01
N30	Cα	53.32	-
N30	Cβ	40.09	38.97 ± 0.01
S31	Cα	56.64	58.45 ± 0.01
S31	Cβ	61.96	63.80 ± 0.01
S32	Cα	60.18	58.69 ± 0.01
S32	Cβ	64.01	63.73 ± 0.01
E33	Cα	56.15	56.88 ± 0.02
E33	Cβ	30.34	30.19 ± 0.01
E33	Cγ	36.28	36.12 ± 0.01
G34	Cα	45.92	45.27 ± 0.01
D35	Cα	55.42	54.43 ± 0.01
D35	Cβ	41.19	40.83 ± 0.01
W36	Cα	55.84	57.99 ± 0.02

Residue	Nucleus	ϖ_G (ppm)	ϖ_E (ppm)
W36	Cβ	31.44	29.32 ± 0.01
W37	Cα	52.77	57.82 ± 0.02
W37	Cβ	32.25	29.12 ± 0.01
E38	Cα	56.35	56.95 ± 0.02
E38	Cβ	30.76	30.30 ± 0.02
E38	Cγ	36.68	36.20 ± 0.01
A39	Cα	51.07	52.76 ± 0.02
A39	Cβ	25.82	18.99 ± 0.01
R40	Cα	53.62	56.18 ± 0.02
R40	Cβ	33.76	30.81 ± 0.01
R40	Cγ	27.11	26.89 ± 0.03
R40	Cδ	43.50	43.28 ± 0.01
S41	Cα	57.60	-
S41	Cβ	63.28	63.52 ± 0.03
L42	Cα	56.76	55.44 ± 0.01
L42	Cβ	40.46	42.39 ± 0.01
L42	Cγ	28.82	27.00 ± 0.01
L42	Cδ1	25.33	25.05 ± 0.01
L42	Cδ2	23.51	23.28 ± 0.01
T43	Cα	65.71	61.96 ± 0.01
T43	Cβ	69.09	69.69 ± 0.01
T43	Cγ2	22.23	21.58 ± 0.01
T44	Cα	61.74	62.01 ± 0.02
T44	Cβ	70.97	69.87 ± 0.02
T44	Cγ2	21.71	21.52 ± 0.01
G45	Cα	45.71	45.32 ± 0.02
E46	Cα	56.61	56.44 ± 0.03
E46	Cβ	31.36	30.54 ± 0.01
E46	Cγ	36.45	36.30 ± 0.03
T47	Cα	61.08	61.87 ± 0.02
T47	Cβ	70.51	69.85 ± 0.01
T47	Cγ2	21.29	21.58 ± 0.01
A48	Cα	51.83	52.22 ± 0.01
A48	Cβ	21.12	19.51 ± 0.01

Residue	Nucleus	ϖ_G (ppm)	ϖ_E (ppm)
Y49	Cα	58.33	57.74 ± 0.02
Y49	Cβ	39.82	38.90 ± 0.01
I50	Cα	57.31	57.86 ± 0.01
I50	Cβ	39.98	39.09 ± 0.01
I50	Cγ1	26.51	26.95 ± 0.01
I50	Cγ2	18.79	17.03 ± 0.01
I50	Cδ1	13.99	12.64 ± 0.01
P51	Cα	61.14	63.04 ± 0.01
P51	Cβ	30.16	32.14 ± 0.01
P51	Cγ	26.71	27.25 ± 0.01
P51	Cδ	49.95	50.88 ± 0.02
S52	Cα	60.17	58.59 ± 0.06
S52	Cβ	60.81	-
N53	Cα	53.48	53.08 ± 0.02
N53	Cβ	36.48	38.55 ± 0.01
Y54	Cα	58.97	58.50 ± 0.02
Y54	Cβ	39.76	39.07 ± 0.03
V55	Cα	58.36	61.31 ± 0.01
V55	Cβ	36.87	33.26 ± 0.01
V55	Cγ1	21.47	21.03 ± 0.01
V55	Cγ2	18.54	20.57 ± 0.01
A56	Cα	49.93	50.32 ± 0.02
A56	Cβ	21.57	17.84 ± 0.01
P57	Cα	62.82	62.92 ± 0.07
P57	Cβ	31.84	32.10 ± 0.01
P57	Cγ	27.30	27.17 ± 0.03
P57	Cδ	50.40	50.28 ± 0.02
V58	Cα	62.88	62.12 ± 0.01
V58	Cβ	32.89	32.75 ± 0.03
V58	Cγ1	21.44	21.15 ± 0.01
V58	Cγ2	21.49	20.18 ± 0.01
D59	Cα	54.19	54.05 ± 0.03
D59	Cβ	40.82	41.16 ± 0.01
R60	Cα	57.09	57.05 ± 0.19

Residue	Nucleus	ϖ_G (ppm)	ϖ_E (ppm)
R60	Cβ	31.15	31.56 ± 0.01
R60	Cγ	24.43	26.73 ± 0.01
R60	Cδ	43.52	43.30 ± 0.01

[a]Ground state chemical shifts are obtained from direct measurement of spectra recorded with scheme c of Supplementary Figure 1. Excited state chemical shifts are generated from fits of CEST profiles, as described in the Materials and methods.

Supplementary Table 3. Ground (ϖ_G) and excited (ϖ_E) state chemical shifts of the L24A FF domain, 25°C.[a]

Residue	Nucleus	ϖ_G (ppm)	ϖ_E (ppm)
S2	Cα	58.32	58.05±0.02
S2	Cα	58.32	58.05±0.02
S2	Cα	58.32	58.05±0.02
S2	Cβ	63.96	63.72±0.03
Q3	Cα	53.76	53.49±0.02
Q3	Cβ	28.95	29.26±0.03
Q3	Cγ	33.48	33.72±0.03
P4	Cα	63.03	62.80±0.02
P4	Cβ	32.14	32.39±0.03
P4	Cγ	27.40	27.16±0.06
P4	Cδ	50.69	50.49±0.02
A5	Cα	52.35	52.12±0.02
A5	Cβ	19.25	19.45±0.02
K6	Cα	56.16	-
K6	Cβ	33.21	33.47±0.03
K6	Cγ	24.73	24.98±0.04
K6	Cδ	29.14	28.79±0.02
K6	Cε	42.14	41.89±0.03
K7	Cβ	33.25	33.53±0.04
K7	Cγ	24.77	25.05±0.04
K7	Cδ	29.02	28.83±0.05
K7	Cε	42.16	41.78±0.01
T8	Cα	61.51	61.26±0.02
T8	Cβ	70.06	69.78±0.02
T8	Cγ2	21.54	-
Y9	Cα	57.37	57.70±0.02
Y9	Cβ	39.55	39.05±0.04
T10	Cα	60.69	61.43±0.01
T10	Cβ	70.93	69.96±0.01
T10	Cγ2	21.15	21.47±0.02
W11	Cα	56.54	57.62±0.05

Residue	Nucleus	ϖ_G (ppm)	ϖ_E (ppm)
W11	Cβ	29.46	29.88±0.06
N12	Cα	54.60	54.04±0.08
N12	Cβ	40.72	39.29±0.01
T13	Cα	59.37	-
T13	Cβ	72.66	70.86±0.09
T13	Cγ2	21.82	22.01±0.03
K14	Cα	58.57	58.00±0.01
K14	Cβ	31.10	32.15±0.04
K14	Cγ	24.47	25.05±0.02
K14	Cδ	28.15	-
K14	Cε	41.58	41.46±0.17
E15	Cα	59.86	58.47±0.01
E15	Cβ	28.94	29.55±0.03
E15	Cγ	36.40	36.09±0.03
E16	Cα	59.13	58.18±0.02
E16	Cβ	30.69	30.09±0.03
E16	Cγ	37.05	36.48±0.03
A17	Cα	55.10	53.88±0.01
A17	Cβ	18.40	18.67±0.02
K18	Cα	60.24	58.40±0.01
K18	Cβ	32.78	32.43±0.05
K18	Cγ	26.17	25.16±0.03
K18	Cδ	29.98	29.31±0.02
K18	Cε	41.76	42.16±0.02
Q19	Cα	58.72	57.47±0.02
Q19	Cβ	28.11	28.64±0.04
Q19	Cγ	33.35	33.63±0.03
A20	Cα	55.03	53.96±0.03
A20	Cβ	17.92	18.68±0.01
F21	Cα	62.12	59.47±0.01
F21	Cβ	40.51	39.17±0.06
K22	Cα	60.29	58.51±0.01
K22	Cβ	32.05	32.62±0.05
K22	Cγ	26.70	25.04±0.04
K22	Cδ	29.91	29.31±0.01

Residue	Nucleus	ϖ_G (ppm)	ϖ_E (ppm)
K22	Cε	41.90	42.53±0.02
E23	Cα	59.22	58.01±0.01
E23	Cβ	28.95	29.61±0.06
E23	Cγ	36.56	36.02±0.02
A24	Cα	55.60	53.99±0.01
A24	Cβ	17.33	18.49±0.01
L25	Cα	57.63	56.54±0.01
L25	Cβ	40.41	41.94±0.06
L25	Cγ	25.64	26.47±0.06
L25	Cδ1	27.77	25.22±0.01
L25	Cδ2	24.95	24.96±4.44
K26	Cα	59.20	57.81±0.02
K26	Cβ	33.15	32.66±0.03
K26	Cγ	25.03	24.72±0.06
K26	Cδ	29.68	29.81±0.12
E27	Cα	59.52	57.08±0.01
E27	Cβ	29.73	30.16±0.03
E27	Cγ	37.21	36.14±0.01
K28	Cα	54.91	56.09±0.02
K28	Cβ	31.12	31.63±0.07
K28	Cγ	26.14	25.04±0.02
K28	Cδ	27.74	28.73±0.02
K28	Cε	42.62	42.06±0.02
R29	Cα	55.95	55.63±0.02
R29	Cβ	26.41	30.10±0.08
R29	Cγ	27.27	26.45±0.03
R29	Cδ	43.50	43.79±0.02
V30	Cα	61.85	59.72±0.01
V30	Cβ	32.19	32.67±0.03
V30	Cγ1	20.89	21.21±0.02
V30	Cγ2	22.70	20.59±0.01
P31	Cα	63.24	62.97±0.04
P31	Cβ	32.87	32.30±0.02
P31	Cγ	27.72	27.42±0.04
P31	Cδ	51.46	51.57±0.44

Residue	Nucleus	ϖ_G (ppm)	ϖ_E (ppm)
S32	Cα	60.99	59.32±0.02
S32	Cβ	63.00	-
N33	Cα	51.71	53.06±0.12
N33	Cβ	37.69	38.40±0.03
A34	Cα	52.60	52.96±0.01
A34	Cβ	19.65	19.73±0.26
S35	Cα	56.77	-
S35	Cβ	65.48	64.17±0.05
W36	Cα	59.96	59.71±0.05
W36	Cβ	28.74	29.25±0.10
E37	Cα	60.79	59.26±0.01
E37	Cβ	28.67	29.36±0.04
E37	Cγ	37.26	36.40±0.01
Q38	Cα	58.20	57.82±0.02
Q38	Cβ	28.64	28.88±0.09
Q38	Cγ	33.62	33.91±0.04
A39	Cα	55.01	54.37±0.01
A39	Cβ	19.98	18.68±0.02
M40	Cα	58.18	56.70±0.01
M40	Cβ	31.71	-
M40	Cγ	31.44	32.20±0.12
M40	Cε	18.04	17.16±0.01
K41	Cα	58.93	58.23±0.01
K41	Cβ	32.22	32.54±0.02
K41	Cγ	25.34	25.07±0.04
K41	Cε	42.04	42.31±0.03
M42	Cα	58.52	57.07±0.01
M42	Cβ	33.50	-
M42	Cγ	33.36	-
M42	Cε	17.57	17.64±0.25
I43	Cα	61.48	62.67±0.01
I43	Cβ	40.06	38.58±0.02
I43	Cγ1	25.48	27.77±0.04
I43	Cγ2	17.63	17.83±0.03
I43	Cδ1	15.58	13.25±0.01

Residue	Nucleus	ϖ_G (ppm)	ϖ_E (ppm)
I44	Cα	63.12	62.53±0.01
I44	Cβ	37.64	38.29±0.02
I44	Cγ1	28.91	27.65±0.01
I44	Cγ2	16.26	17.58±0.01
I44	Cδ1	14.40	13.41±0.01
N45	Cα	52.73	-
N45	Cβ	38.74	39.10±0.04
D46	Cα	51.70	51.96±0.16
D46	Cβ	44.19	42.91±0.05
P47	Cα	65.32	64.37±0.01
P47	Cβ	32.78	32.19±0.02
P47	Cγ	27.91	27.16±0.01
P47	Cδ	51.26	50.97±0.07
R48	Cα	57.69	57.35±0.03
R48	Cγ	27.31	-
R48	Cδ	42.13	43.45±0.06
Y49	Cα	61.26	58.25±0.01
Y49	Cβ	38.72	39.17±0.08
S50	Cα	58.33	60.19±0.02
S50	Cβ	63.52	63.23±0.02
A51	Cα	54.81	53.85±0.01
A51	Cβ	18.07	18.70±0.01
L52	Cα	51.69	56.22±0.02
L52	Cβ	42.28	41.71±0.07
L52	Cγ	25.79	26.89±0.08
L52	Cδ1	26.39	25.21±0.04
L52	Cδ2	22.99	23.56±0.01
A53	Cα	54.55	53.67±0.01
A53	Cβ	20.05	18.79±0.01
K54	Cα	55.58	56.94±0.01
K54	Cβ	33.51	-
K54	Cγ	25.34	25.46±0.24
K54	Cδ	29.20	-
K54	Cε	42.08	-
L55	Cα	58.71	56.00±0.02

Residue	Nucleus	ϖ_G (ppm)	ϖ_E (ppm)
L55	Cβ	41.18	42.18±0.02
L55	Cγ	27.04	27.29±0.07
L55	Cδ1	23.79	25.16±0.01
L55	Cδ2	24.91	23.51±0.01
S56	Cα	61.12	-
S56	Cβ	61.29	-
E57	Cα	58.62	57.01±0.02
E57	Cβ	30.23	30.79±0.06
E57	Cγ	37.17	36.16±0.02
K58	Cα	59.65	56.72±0.15
K58	Cβ	34.34	32.75±0.04
K58	Cγ	25.40	24.90±0.09
K58	Cδ	30.74	29.01±0.03
K58	Cε	42.55	42.07±0.04
K59	Cα	60.29	56.83±0.01
K59	Cβ	32.03	32.81±0.04
K59	Cγ	25.54	24.82±0.02
K59	Cδ	29.24	28.87±0.06
K59	Cε	41.44	42.10±0.02
Q60	Cα	59.19	56.17±0.01
Q60	Cβ	28.48	29.43±0.01
Q60	Cγ	34.02	34.24±0.03
A61	Cα	55.06	52.70±0.03
A61	Cβ	18.63	19.22±0.01
F62	Cα	60.52	58.17±0.02
F62	Cβ	39.49	39.83±0.07
N63	Cα	56.41	53.29±0.02
N63	Cβ	37.73	38.92±0.03
A64	Cα	54.81	52.94±0.01
A64	Cβ	18.21	19.06±0.01
Y65	Cα	60.58	58.05±0.01
Y65	Cβ	38.88	38.55±0.10
K66	Cα	59.94	56.25±0.01
K66	Cβ	32.06	33.18±0.04
K66	Cγ	24.57	24.86±0.04

Residue	Nucleus	ϖ_G (ppm)	ϖ_E (ppm)
K66	Cδ	29.61	29.10±0.02
K66	Cε	41.74	41.40±0.04
V67	Cα	63.50	62.51±0.01
V67	Cβ	31.91	32.66±0.01
V67	Cγ1	21.23	21.42±0.03
V67	Cγ2	20.89	21.08±0.03
Q68	Cα	56.69	55.91±0.01
Q68	Cγ	33.93	34.07±0.10
T69	Cα	62.56	61.88±0.01
T69	Cβ	69.66	69.37±0.03
E70	Cα	56.78	57.03±0.02
E70	Cβ	30.10	29.93±0.06
E70	Cγ	35.95	35.66±0.02
K71	Cα	57.71	57.48±0.02
K71	Cβ	33.67	33.91±0.02

[a]Ground state chemical shifts are obtained from direct measurement of spectra recorded with scheme c of Supplementary Figure 1. Excited state chemical shifts are generated from fits of CEST profiles, as described in the Materials and methods.

REFERENCES

1. McConnell, H. M. (1958). Reaction rates by nuclear magnetic resonance. *J. Chem. Phys.* **28**, 430-431.
2. Vuister, G. W. & Bax, A. (1992). Resolution enhancement and spectral editing of uniformly ^{13}C-enriched proteins by homonuclear broadband ^{13}C decoupling. *J. Magn. Reson.* **98**, 428-435.
3. Santoro, J. & King, G. C. (1992). A constant-time 2D overbodenhausen experiment for inverse correlation of isotopically enriched species. *J. Magn. Reson.* **97**, 202-207.
4. Levitt, M. & Freeman, R. (1978). NMR population inversion using a composite pulse. *J. Magn. Reson.* **33**, 473-476.
5. Vallurupalli, P., Bouvignies, G. & Kay, L. E. (2012). Studying 'Invisible' Excited Protein States in Slow Exchange with a Major Conformation. *J. Am. Chem. Soc.*
6. Shaka, A. J., Keeler, J., Frenkiel, T. & Freeman, R. (1983). An improved sequence for broadband decoupling: WALTZ-16. *J. Magn. Reson.* **52**, 335-338.
7. Geen, H. & Freeman, R. (1991). Band-selective radiofrequency pulses. *J. Magn. Reson.* **93**, 93-141.
8. Matsuo, H., Kupce, E., Li, H. & Wagner, G. (1996). Increased sensitivity in HNCA and HNCOCA experiments by selective Cb decoupling. *J. Magn. Reson.* **113**, 91-96.
9. Kupce, E. & Wagner, G. (1996). Multisite Band-Selective Decoupling in Proteins. *J. Magn. Reson. B* **110**, 309-312.
10. Zhang, S. M. & Gorenstein, D. G. (1998). Bloch-Siegert shift compensated and cyclic irradiation sidebands eliminated, double-adiabatic homonuclear decoupling for C-13 and N-15 labeled proteins. *J. Magn. Reson.* **132**, 81-87.
11. Kupce, E. & Freeman, R. (1995). Stretched adiabatic pulses for broadband spin inversion. *J. Magn. Reson. Series A* **117**, 246-256.
12. Shaka, A. J., Barker, P. B. & Freeman, R. (1985). Computer-optimized decoupling scheme for wideband applications and low-level operation. *J. Magn. Reson.* **64**, 547-552.
13. Marion, D., Ikura, M., Tschudin, R. & Bax, A. (1989). Rapid recording of 2D NMR spectra without phase cycling. Application to the study of hydrogen exchange in proteins. *J. Magn. Reson.* **85**, 393-399.
14. Kay, L. E., Keifer, P. & Saarinen, T. (1992). Pure absorption gradient enhanced heteronuclear single quantum correlation spectroscopy with improved sensitivity. *J. Am. Chem. Soc.* **114**, 10663-10665.
15. Schleucher, J., Sattler, M. & Griesinger, C. (1993). Coherence selection by gradients without signal attenuation: Application to the three-dimensional HNCO experiment. *Angew. Chem. Int. Ed. Engl.* **32**, 1489-1491.
16. Sattler, M., Schleucher, J. & Griesinger, C. (1999). Heteronuclear multidimensional NMR experiments for the structure determination of proteins in solution employing pulsed field gradients. *Prog. Nucl. Magn. Reson. Spectrosc.* **34**, 93-158.
17. Shaka, A. J., Lee, C. J. & Pines, A. (1988). Iterative schemes for bilinear operators-Application to spin decoupling. *J. Magn. Reson.* **77**, 274-293.
18. Abragam, A. (1961). *Principles of Nuclear Magnetism*, Clarendon Press, Oxford.

19. Kupce, E. & Freeman, R. (1996). Optimized adiabatic pulses for wideband spin inversion. *J. Magn. Reson. Ser. A*. **118**, 299-303.
20. Press, W. H., Flannery, B. P., Teukolsky, S. A. & Vetterling, W. T. (1988). *Numerical Recipes in C.*, Cambridge University Press, Cambridge.